NASA
Technical
Memorandum

NASA TM - 108411

DESIGN OF MULTIPLE-PLY LAMINATED COMPOSITE TAPERED BEAMS

By P. Rodriguez

Structures and Dynamics Laboratory
Science and Engineering Directorate

June 1993

National Aeronautics and
Space Administration

George C. Marshall Space Flight Center

REPORT DOCUMENTATION PAGE

Form Approved
OMB No. 0704-0188

1. AGENCY USE ONLY *(Leave blank)*	2. REPORT DATE	3. REPORT TYPE AND DATES COVERED
	June 1993	Technical Memorandum

4. TITLE AND SUBTITLE

Design of Multiple-Ply Laminated Composite Tapered Beams

5. FUNDING NUMBERS

6. AUTHOR(S)

P. Rodriguez

7. PERFORMING ORGANIZATION NAME(S) AND ADDRESS(ES)

George C. Marshall Space Flight Center
Marshall Space Flight Center, Alabama 35812

8. PERFORMING ORGANIZATION REPORT NUMBER

9. SPONSORING/MONITORING AGENCY NAME(S) AND ADDRESS(ES)

National Aeronautics and Space Administration
Washington, DC 20546

10. SPONSORING/MONITORING AGENCY REPORT NUMBER

NASA TM-108411

11. SUPPLEMENTARY NOTES

Prepared by Structures and Dynamics Laboratory, Science and Engineering Directorate

12a. DISTRIBUTION/AVAILABILITY STATEMENT

Unclassified—Unlimited

12b. DISTRIBUTION CODE

13. ABSTRACT *(Maximum 200 words)*

A study of a special case of symmetric laminated composite cantilever beams is presented. The approach models beams that are tapered both in depth and width and investigates the effect of the ply layup angle and the ply taper on bending and interlaminar shearing stresses. For the determination of stresses and deflections, the beam stiffness matrices are expressed as linear functions of the beam length. Using classical lamination theory (CLT) the stiffness matrices are determined and assembled at strategic locations along the length of the beam. They are then inverted and necessary stiffness parameters are obtained numerically and extracted for determination of design information at each location chosen. Several ply layup configurations are investigated, and design considerations are presented based on the findings. Finally, recommendations for the design of these beams are presented, and a means for anticipating the location of highest stresses is offered.

14. SUBJECT TERMS

Filamentary Composites, Tapered Beams, Interlaminar Stresses, Classical Lamination Theory

15. NUMBER OF PAGES

40

16. PRICE CODE

NTIS

17. SECURITY CLASSIFICATION OF REPORT	18. SECURITY CLASSIFICATION OF THIS PAGE	19. SECURITY CLASSIFICATION OF ABSTRACT	20. LIMITATION OF ABSTRACT
Unclassified	Unclassified	Unclassified	Unlimited

ACKNOWLEDGMENTS

The author would like to express his sincere appreciation to Mrs. Peggy L. Frazier for her enthusiasm and patience in proofreading, typing, and retyping the manuscript for this work. Acknowledgment is also given to Mr. Stan S. Smeltzer for his many constructive suggestions during his review of the manuscript.

TABLE OF CONTENTS

LIST OF ILLUSTRATIONS

LIST OF ILLUSTRATIONS (Continued)

LIST OF TABLES

LIST OF SYMBOLS

A_{ij}	extensional stiffness matrix
D_{ij}	bending stiffness matrix
D_{ij}^*	inverted bending stiffness matrix
dx, dw, dt	differential elements
k	ply or lamina number
L	beam length
m, n	dummy counters
M_x	applied moment (per unit width)
P	applied load
$\bar{Q}_{ij}$	transformed reduced stiffness matrix
$(QD_x)^{(k)}$	$\bar{Q}_{11}^{(k)}D_{11}^*+\bar{Q}_{12}^{(k)}D_{12}^*+\bar{Q}_{16}^{(k)}D_{16}^*$
t	thickness
t_e	thickness at free end of beam
t_o	thickness at fixed end of beam
t_1	$\frac{t_e-t_o}{L}$
t_2	t_o
$t(x)$	$t_1 x+t_2$
w	beam deflection, beam width
w_e	width at free end of beam
w_o	width at fixed end of beam
w_1	$\frac{w_e-w_o}{L}$
w_2	w_o

LIST OF SYMBOLS (Continued)

$w(x)$	$w_1 x+w_2$
x	length coordinate
y	width coordinate
z	thickness coordinate
γ_j	beam curvatures
Γ_j	constants
λ_j	constants
ε_j	strains
ρ	material density
σ_j	stresses

TECHNICAL MEMORANDUM

DESIGN OF A MULTIPLE-PLY LAMINATED COMPOSITE TAPERED BEAMS

INTRODUCTION

In a recent paper,[1] the author developed a method based on classical lamination theory (CLT) and a linear elastic solution for the optimum design of a special class of laminated cantilever beams. The method, developed for beams which are tapered in width and thickness, expresses the extensional and bending stiffness matrices as functions of the linearly varying thickness along the length of the beam. The method also expresses the bending moment per unit width as a function of the linearly varying width along the length. The special case analyzed was the case of a four-ply laminated beam where the two outermost plies were tapered. The present work extends the original research to laminated beams of multiple plies.

Findings of the present research include very high dependence of the interlaminar shearing stresses on the difference in layup angle between a tapering ply and the one adjacent to it. Other findings are that due to the strong dependence of the bending stresses on the stiffness parameter D_{11}, the location of the highest bending, and consequently transverse (interlaminar) shear stresses, can be determined by knowing the shape of the D_{11} curve as a function of beam length. It is also found that in some instances, stresses can be reduced by over 50 percent by simply interchanging plies within the design laminate with very small changes in the corresponding beam stiffness (less than 8 percent). The work presented here serves as a precursor to future research where the effects of the time-dependent behavior of the viscoelastic matrix of the composite material is included. As the use of composite materials becomes more widespread for space applications, such as for the Advanced X-Ray Astrophysics Facility-S (AXAF-S) project, design engineers will need more knowledge of long-term structural behavior of composite systems.

LAMINATED BEAM EQUATIONS

Following the CLT, the assembled extensional and bending stiffness matrices for an orthotropic material can be expressed as,

$$[A_{ij}] = \begin{bmatrix} A_{11} & A_{12} & A_{16} \\ A_{21} & A_{22} & A_{26} \\ A_{61} & A_{62} & A_{66} \end{bmatrix} \tag{1}$$

$$[D_{ij}] = \begin{bmatrix} D_{11} & D_{12} & D_{16} \\ D_{21} & D_{22} & D_{26} \\ D_{61} & D_{62} & D_{66} \end{bmatrix} \tag{2}$$

The individual terms of equations (1) and (2) can be obtained following the procedure prescribed by the CLT with the exception that only the innermost plies are not tapered and their thickness does not depend on x. The outer plies are tapered and must be expressed as functions of x. In practice, plies cannot be tapered. In this report, the length of one tapered ply is equivalent to the length of several stepped plies which simulate the slope of the desired taper (figs. 1 and 1a). With this in mind, one can write,

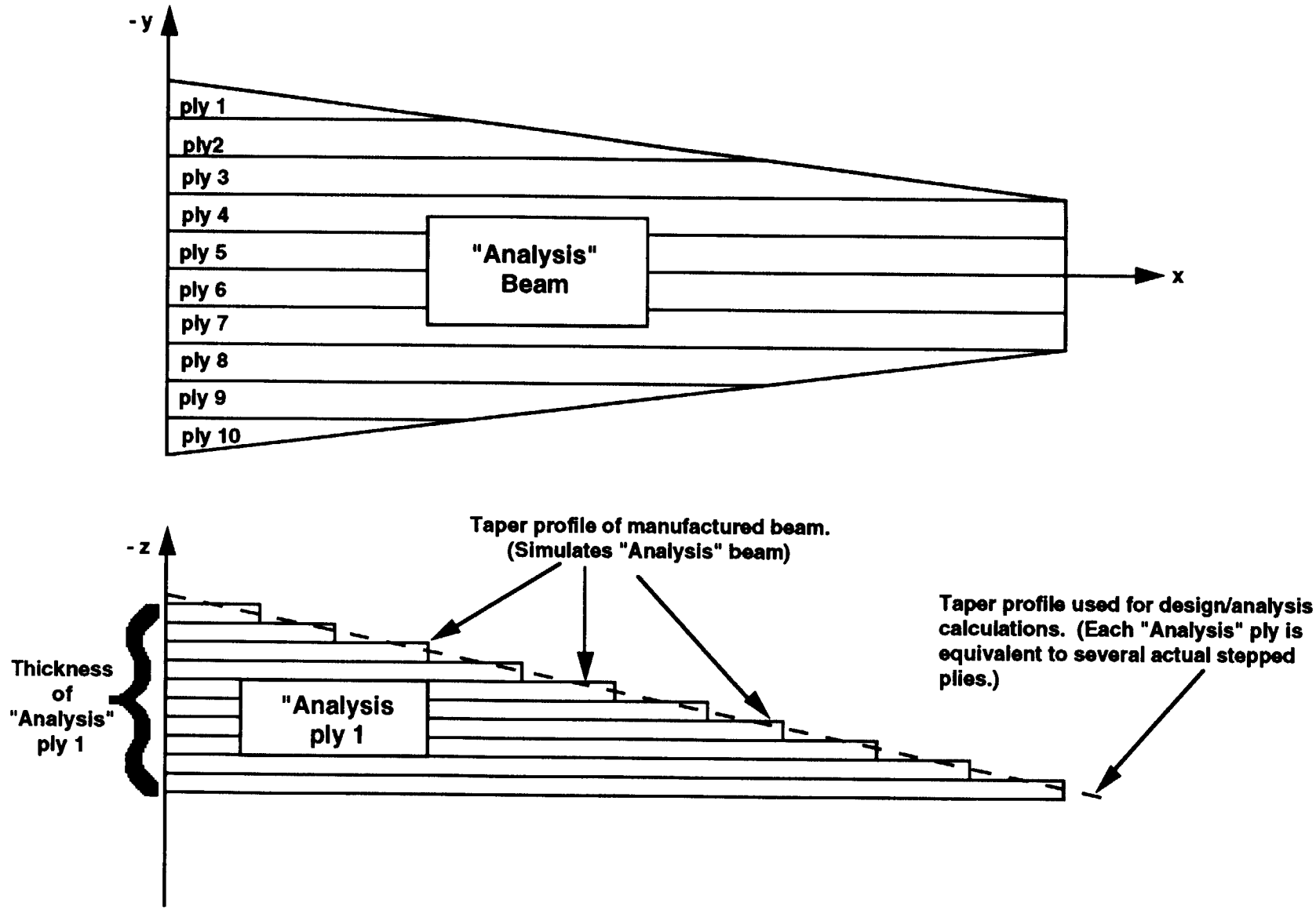

Figure 1. Laminated tapered beam configuration.

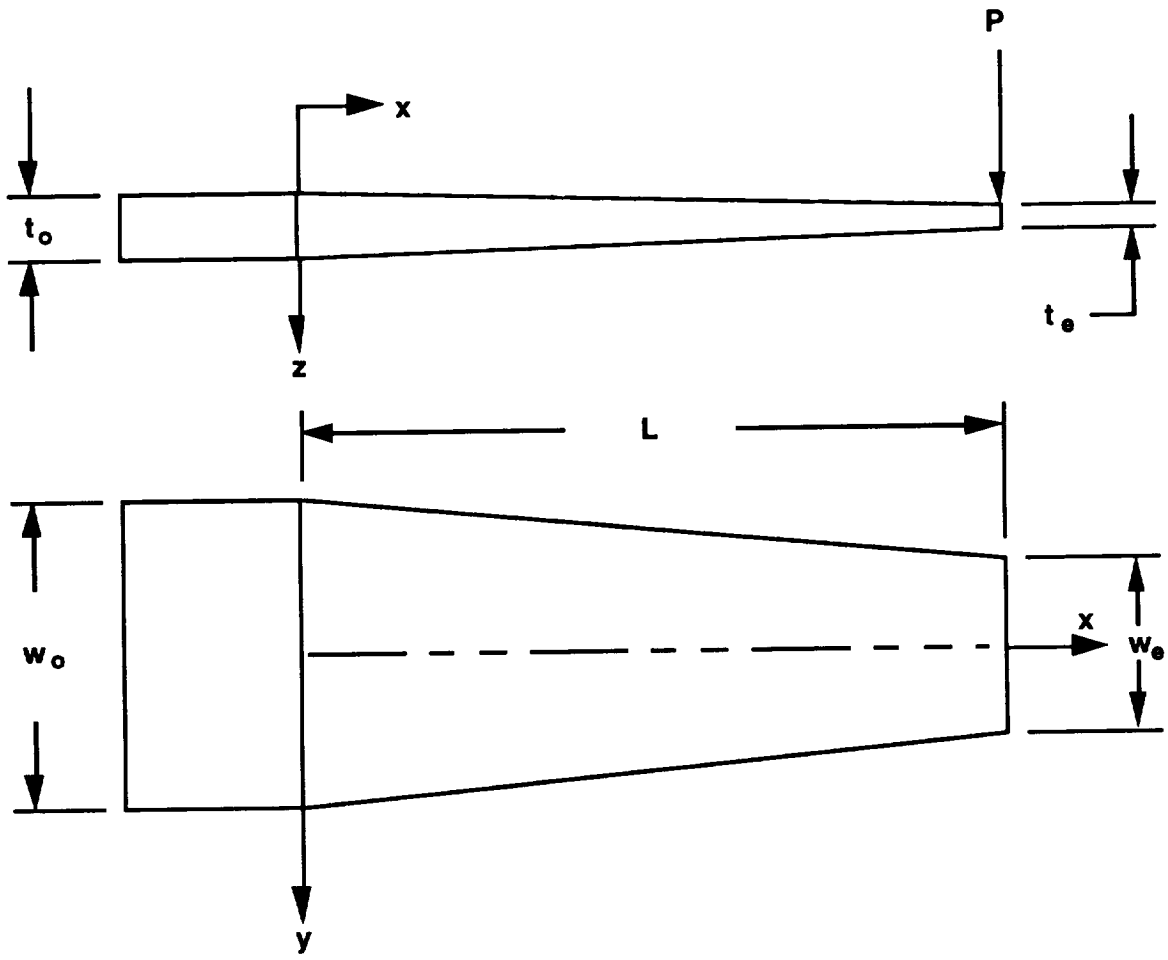

Figure 1*a*. Tapered beam dimensions and geometry.

$$A_{ij} = \sum_{k=k_m}^{k_n} \bar{Q}_{ij}^{(k)}(z_k - z_{k-1}) + \sum_{k=k_n}^{n} \bar{Q}_{ij}^{(k)}\left\{z_k - \left[z_k - t_k\left(1 - \frac{x}{L}\right)\right]\right\} + \sum_{k=k_m}^{m} \bar{Q}_{ij}^{(k)}\left\{\left[z_{k-1} + t_k\left(1 - \frac{x}{L}\right)\right] - z_{k-1}\right\}, \tag{3}$$

$$D_{ij} = \sum_{k=k_m}^{k_n} \frac{\bar{Q}_{ij}^{(k)}}{3}(z_k^3 - z_{k-1}^3) + \sum_{k=k_n}^{n} \frac{\bar{Q}_{ij}^{(k)}}{3}\left\{z_k^3 - \left[z_k - t_k\left(1 - \frac{x}{L}\right)\right]^3\right\} + \sum_{k=k_m}^{m} \frac{\bar{Q}_{ij}^{(k)}}{3}\left\{\left[z_{k-1} + t_k\left(1 - \frac{x}{L}\right)\right]^3 - z_{k-1}^3\right\}, \tag{4}$$

where $\bar{Q}_{ij}^{(k)}$ are the transformed reduced stiffnesses for the kth ply. Plies k_m through m are the tapered plies at the bottom of the laminate. Plies k_n through n are the tapered plies at the top of the laminate. L represents the length of the ply, and t_k is the thickness of the ply. The validity of equations (3) and (4) is demonstrated in reference 1. One should notice that in equations (3) and (4), the terms

$$\left[z_k - t_k\left(1 - \frac{x}{L}\right)\right] \quad \text{and} \quad \left[z_{k-1} + t_k\left(1 - \frac{x}{L}\right)\right]$$

account for the dependence of the stiffness parameters A_{ij} and D_{ij} on the linear variation of thickness along the length of the beam.

For the cases studied, only pure bending of tapered beams is considered. With this assumption, the extensional stiffness matrix A_{ij} will not play a role in the solution of the beam problem. This would not be the case if the solution were to include the effects of transverse shear deformations.[2] The constitutive relationships for the beam subjected to pure bending can be expressed as,

$$\begin{Bmatrix} \gamma_x \\ \gamma_y \\ \gamma_{xy} \end{Bmatrix} = \begin{bmatrix} D_{11} & D_{12} & D_{16} \\ D_{21} & D_{22} & D_{26} \\ D_{61} & D_{62} & D_{66} \end{bmatrix}^{-1} \begin{Bmatrix} M_x \\ M_y \\ M_{xy} \end{Bmatrix} . \tag{5}$$

For the beams studied, only bending along the longitudinal axis of the beam will be considered. This implies that

$$M_y = M_{xy} = 0 \tag{6}$$

The strain-displacement relationships for the typical Euler-Bernoulli beam are expressed as

$$\gamma_x = -\frac{\partial^2 w}{\partial x^2} , \quad \gamma_y = -\frac{\partial^2 w}{\partial y^2} , \quad \gamma_{xy} = -2\frac{\partial^2 w}{\partial x \partial y} . \tag{7}$$

For beams with large length-to-width ratios, the deflection w can be treated as being a function of x only. Equations (5), (6), and (7) can be combined to express the Euler-Bernoulli beam equation as,

$$\gamma_x = -\frac{d^2 w}{dx^2} = D_{11}^* M_x , \tag{8}$$

where D_{11}^* is the first term of the inverted bending stiffness matrix. Equation (2) can be inverted numerically and a value of D_{11}^* can be obtained at each location of x desired along the length of the beam. Figure 1 shows the beam dimensions and geometry.

Once the values for D_{11}^* are obtained, they can be easily curve fitted with a higher order polynomial to obtain an equation as a function of length. This equation is of the form

$$D_{11}^* = \sum_{i=1}^{n} \Gamma_i x^{i-1} . \tag{9}$$

In the present formulation, a compliance function of the form of equation (9) is calculated for each beam segment with tapered plies. Figures 2 through 4 show the comparison of actual versus curve fitted values of D_{11}^* for three different beam configurations. The material and geometry parameters used are shown in table 1.

Table 1. Material and geometry parameters.

Geometry	Material
w_e – 4.50 in	E_{11} – 21.0E6 lb/in^2
w_o – 6.00 in	E_{22} – 1.7E6 lb/in^2
t_e – 0.50 in	G_{12} – 0.65E6 lb/in^2
t_o – 1.00 in	ν_{12} – 0.31
L – 29.25 in	ν_{21} – 0.017

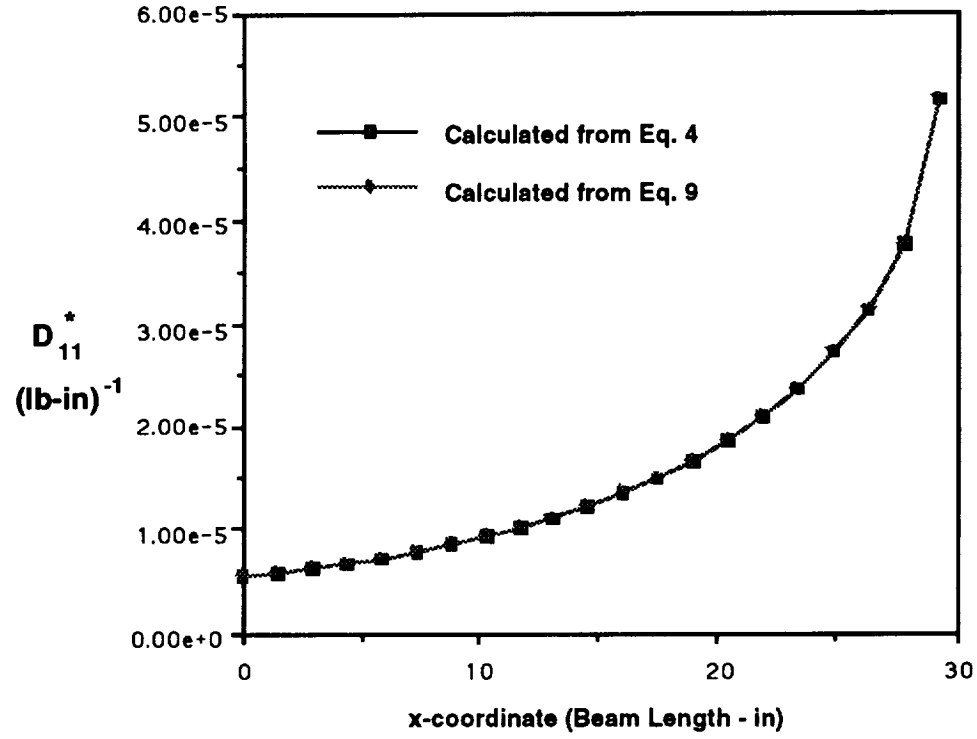

Figure 2. D_{11}^{*} versus length for a four-ply tapered laminated beam $[45/-45]_s$.

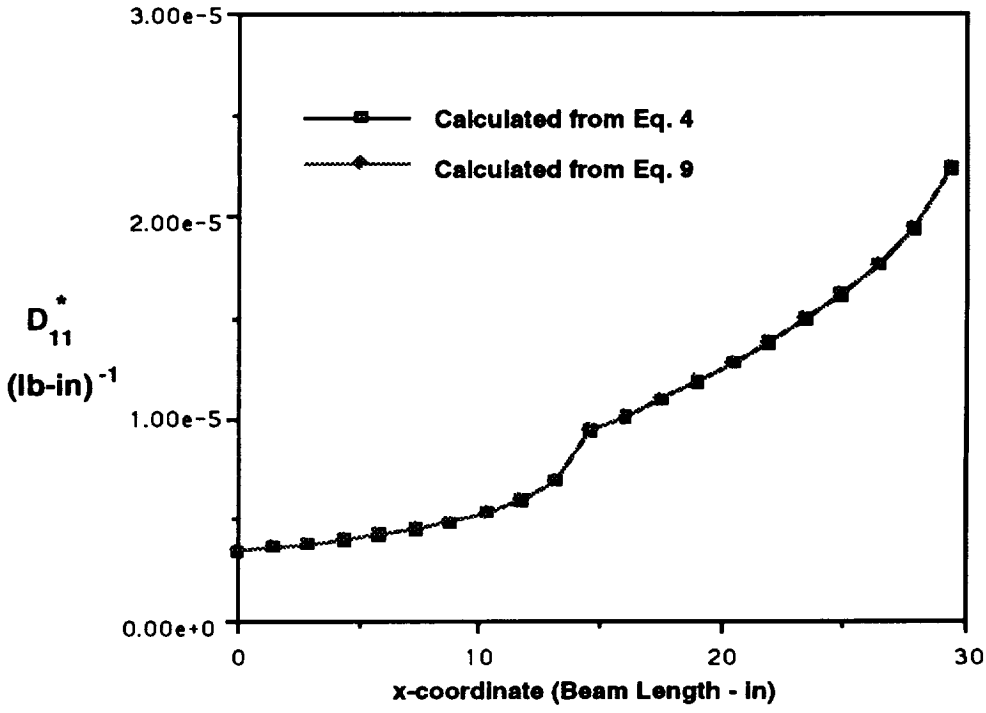

Figure 3. D_{11}^{*} versus length for an eight-ply tapered laminated beam $[90/45/-45/0]_s$.

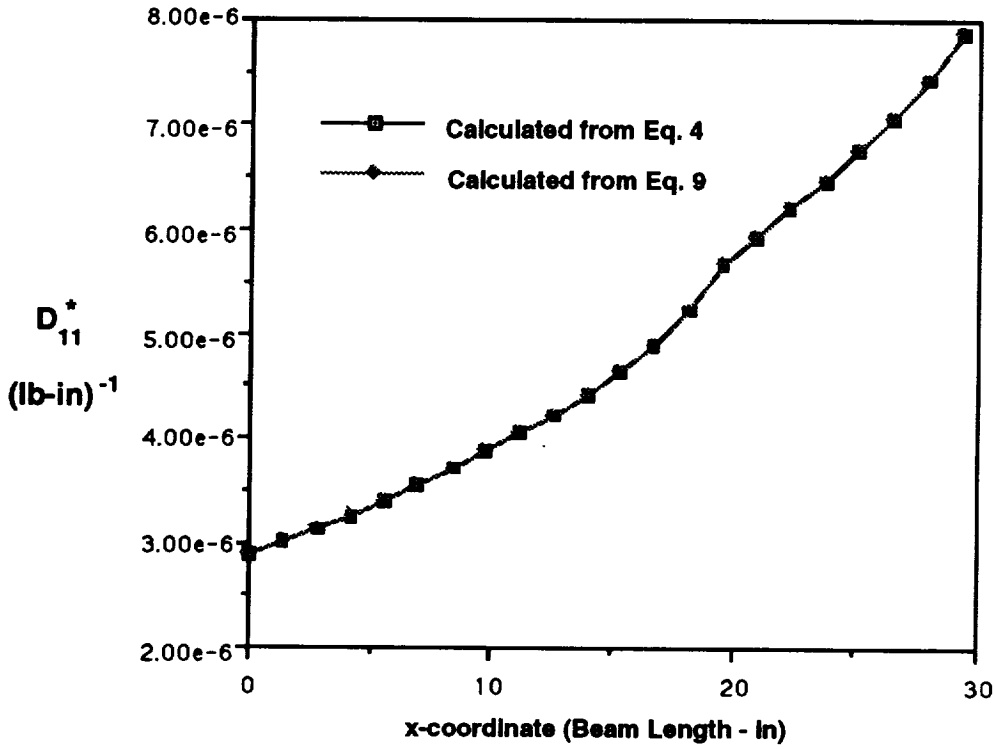

Figure 4. D_{11}^{*} versus length for a 12-ply tapered laminated beam $[90/45/30/15/0/0]_s$.

In equation (8), M_x is the moment per unit width of the beam. Since the width of the beams under study vary linearly as a function of length, this term becomes,

$$M_x = \frac{M}{w_1 x + w_2} = \frac{P(L-x)}{w_1 x + w_2} \ , \tag{10}$$

where

P = applied load at free end = qw_e

q = uniformly distributed applied line load at free end

w_e = beam width at free end

w_o = beam width at fixed end

$$w_1 = \frac{w_e - w_o}{L} \tag{11a}$$

$$w_2 = w_o \tag{11b}$$

substituting equations (9) and (10) into equation (8) leads to

$$-\frac{d^2 w}{dx^2} = \sum_{i=1}^{n} \Gamma_i x^{i-1} \left[\frac{P(L-x)}{w_1 x + w_2} \right] . \tag{12}$$

Performing the required multiplications, equation (12) can be expressed in polynomial form. The resulting equation is easily integrated to obtain slope and deflection values.

$$-\frac{d^2w}{dx^2} = \sum_{i=1}^{n} \lambda_i x^{i-1} , \tag{13}$$

where

$$\lambda_i = \frac{\Gamma_i P(L-x)}{w_1 x + w_2} . \tag{13a}$$

Integrating equation (13), one can obtain values for slope and deflection at any point along the beam. Since the origin of the beams under analysis is located at the base (fixed end) of the beam, the boundary conditions of zero slope and deflection at the fixed end allow the elimination of constants of integration. Thus the slope and deflection of the beam can be expressed as

$$-\frac{dw}{dx} = \sum_{i=1}^{n} \frac{\lambda_i x^i}{i} , \tag{14}$$

$$-w = \sum_{i=1}^{n} \frac{\lambda_i x^{i+1}}{(i+1)i} . \tag{15}$$

Equation (13) represents a smooth continuous function for isotropic materials and for laminated materials where all ply angles are equal. However, because the bending stiffness D_{11} is a function of material properties as well as laminate layup and thickness, marked discontinuities can occur at locations where plies "taper off" to zero. At these locations, the curvature can be discontinuous because it is calculated independently for each beam segment with tapered plies. The physical problem, however, does not allow discontinuities in slope at a location where a ply thickness becomes zero. With this knowledge, the degree of the polynomial in equation (13) can be selected such that the curvature over the length of the entire beam is reasonably approximated. As an example, an eight-ply laminated tapered beam $[90/45/-45/0]_s$, in which only the interior [-45/0/0/-45] plies remain of constant thickness, produces the curvature plot shown in figure 5. Material properties and geometry are shown in table 1. The marked discontinuity occurs because the outermost plies taper down in thickness to zero at this location (x = 14.625 in); and because, again, for each segment, the curvature is calculated independently. Also, at this location the laminate at x greater than 14.625 in only has six plies with the outermost plies having a layup angle of 45°. The laminate at x less than 14.625 in has eight plies with the outermost plies having a layup angle of 90°. Therefore, the beam stiffness is discontinuous at this location (x = 14.625 in). By approximating the curvature with a polynomial, a continuous function which can be easily integrated will be available. Figure 5 also shows the approximation from equation (13). Equation (15) is plotted in figure 6 for the $[90/45/-45/0]_s$ beam. This figure shows the calculated deflected shape of the cantilever beam.

STRESS CALCULATIONS

The stress-strain relationships can be expressed in the classical sense as,

$$\{\sigma_i\}_k = [Q_{ij}]_k \{\{\varepsilon_j\} + z\{\gamma_j\}\} , \tag{16}$$

where the curvatures γ_j are calculated as in equation (13). Since the problems investigated are pure bending, the strains ε_j become negligible, and the stresses become principally functions of the curvatures. Figure 7 shows the normalized bending stresses for a laminated beam where all plies are isotropic.

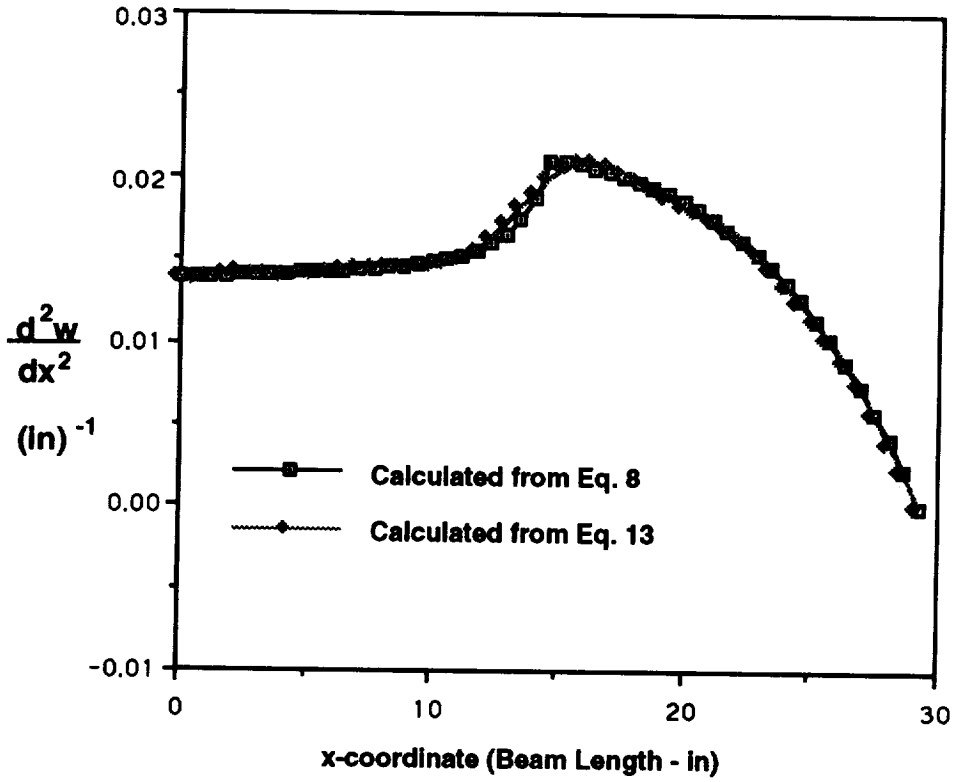

Figure 5. Curvature versus length for an eight-ply laminated beam $[90/45/-45/0]_s$.

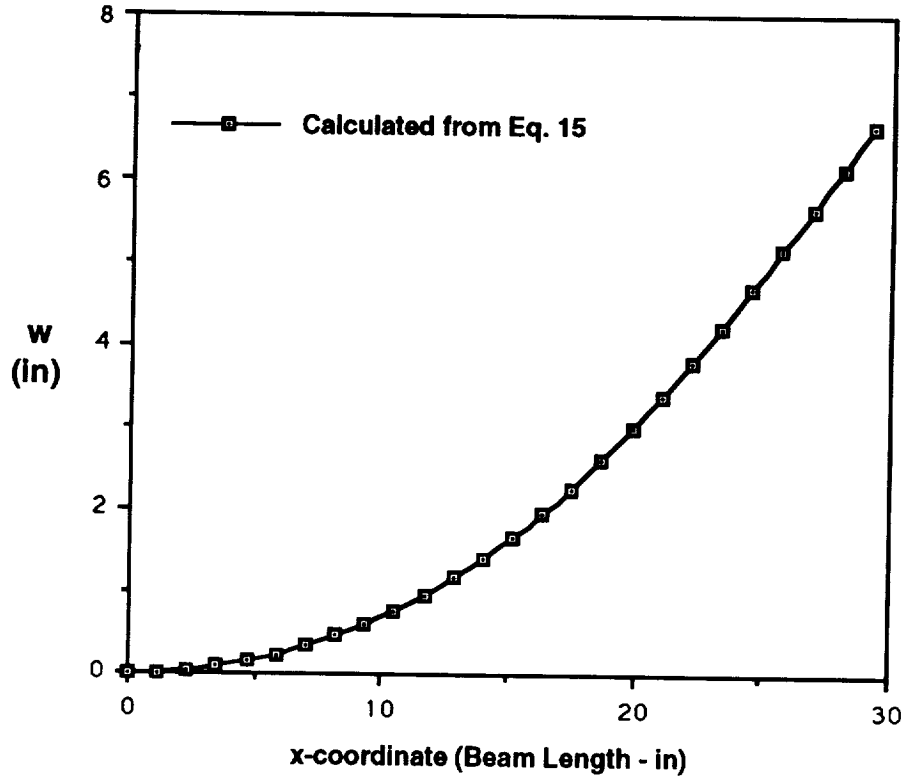

Figure 6. Deflection versus length for an eight-ply laminated beam $[90/45/-45/0]_s$.

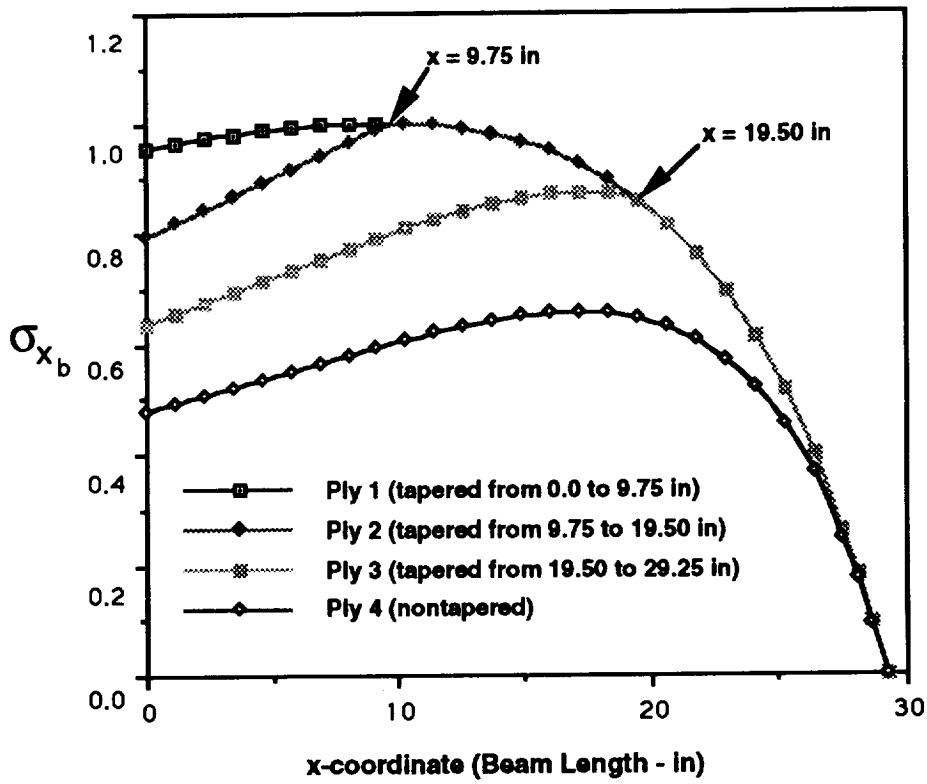

Figure 7. Normalized bending stress versus beam length (multiple isotropic layers).

This serves the purpose of illustrating the stress variation of each ply as a function of length. For this example, the outermost three plies are involved in the tapering of the beam. One should notice how the inner ply stress equals the outer ply stress at the point where the outer ply tapers to zero thickness. In other words, the stresses for plies 1 and 2 are equal at x = 9.75 in; and the stresses for plies 2 and 3 are equal at x = 19.5 in. This is to be expected since the bending stiffness is a continuous function due to the isotropic nature of the plies. One should notice that ply 1 tapers off at x = 9.75 and ply 2 tapers off at x = 19.5 in. The stress for ply 4 is shown to illustrate the variation in stress for a nontapering isotropic ply.

For laminated orthotropic beams in which the bending stiffness is discontinuous at locations where plies taper down to zero thickness, the stresses will also have a marked discontinuity. In some instances, the inner plies may be subjected to higher stresses. Note that for isotropic beams, one would normally expect the highest bending stresses to occur at the outermost fiber. Figure 8 shows the bending stress distribution for a $[90/60/45/30/15/0]_s$ beam. Note that the outermost ply tapers down to zero thickness at x = 9.75 in. At this point, the second ply becomes the outermost ply up to x = 19.50 in. The third ply then becomes the outermost ply for the remainder of the length of the beam.

It is also important to note that the 60° ply begins tapering at x = 9.75 and ends with zero thickness at x = 19.50. Likewise, the 45° ply begins tapering at x = 19.50 and ends with zero thickness at x = 29.25. For this laminated beam the maximum bending stress occurs at x = 19.50 on the 0° ply above the center line of laminate symmetry (not shown in the figure).

The remaining in-plane stresses due to bending σ_y and σ_{xy} are also obtained by substituting equations (5) and (4) into equation (16) and setting $\varepsilon_j = 0$. In this manner, one obtains

$$\sigma_{y_b}^{(k)} = z^{(k)} M_x \left(\bar{Q}_{12}^{(k)} D_{11}^* + \bar{Q}_{22}^{(k)} D_{12}^* + \bar{Q}_{26}^{(k)} D_{16}^* \right) , \tag{17}$$

$$\sigma_{xy_b}^{(k)} = z^{(k)} M_x \left(\bar{Q}_{16}^{(k)} D_{11}^* + \bar{Q}_{26}^{(k)} D_{12}^* + \bar{Q}_{66}^{(k)} D_{16}^* \right) . \tag{18}$$

Figure 9 shows the variation of σ_y for the top plies of the symmetric laminate investigated in figure 8. For an isotropic beam, these stresses would be negligible; but for the orthotropic laminate studied, the maximum σ_y stress is 13,050 lb/in^2. This stress occurs at $x = 9.75$ on the 30° ply above the center line of laminate symmetry. One can also notice that the stress at $x = 19.50$ on the 60° ply has a significantly high compressive σ_y stress. This shows that buckling or compressive failure is possible at locations where one would normally expect to see only tensile stresses (isotropic case). Figure 10 shows the variation of σ_{xy} for the top plies of the beam. Again, for the isotropic beam, one would expect these stresses to be negligible; but for this case, the maximum σ_{xy} stress is 16,850 lb/in^2. This occurs at $x = 9.75$ on the 30° ply.

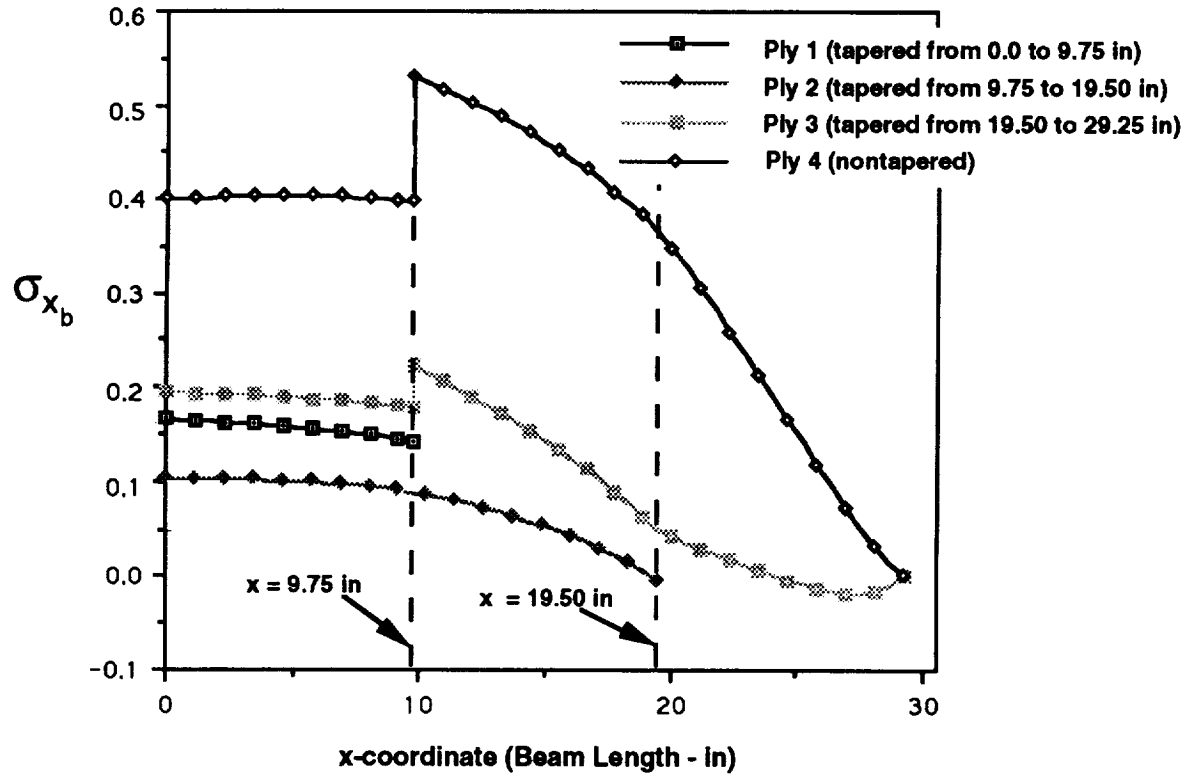

Figure 8. Normalized bending stress versus beam length $[90/60/45/30/15/0]_s$.

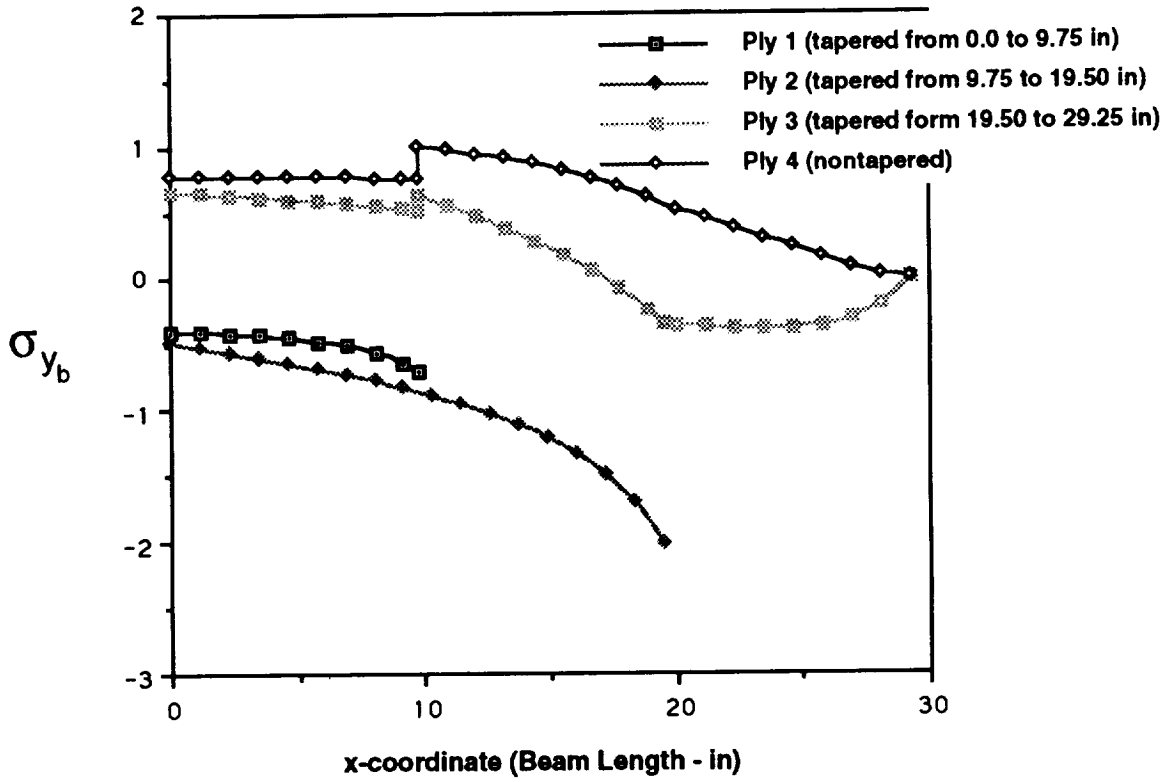

Figure 9. Normalized in-plane stress versus beam length $[90/60/45/30/15/0]_s$.

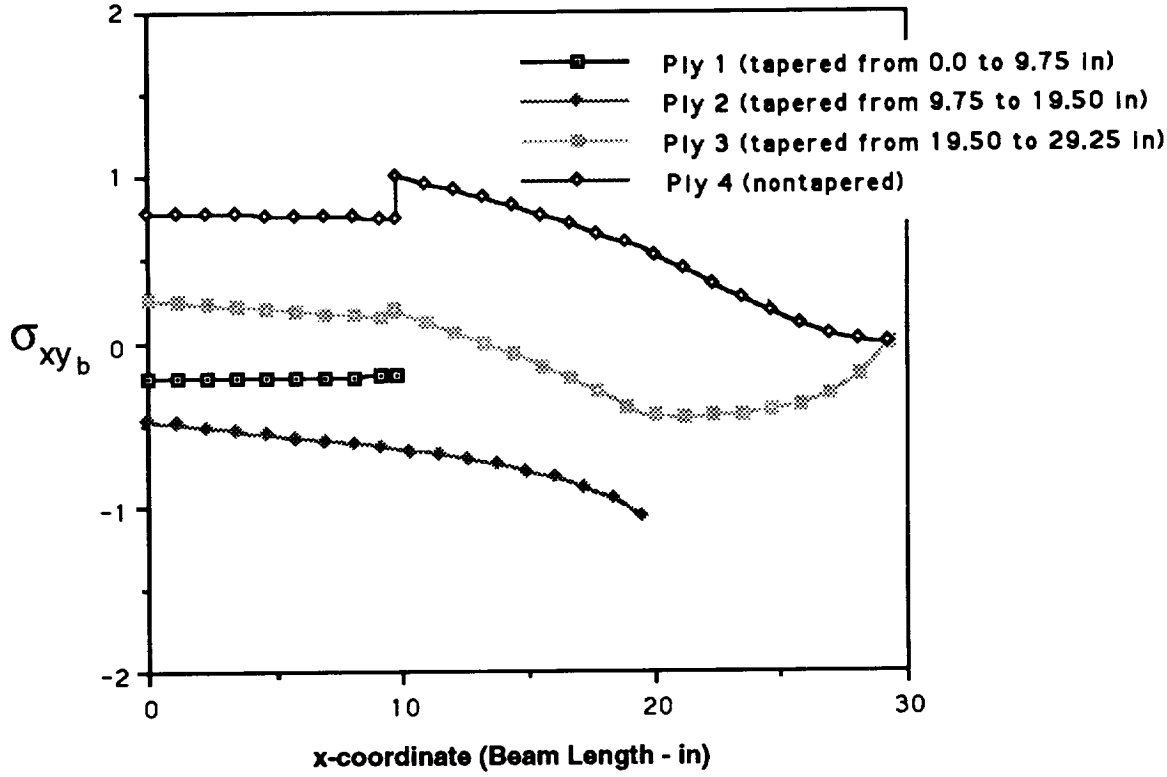

Figure 10. Normalized in-plane shear stress versus beam length $[90/60/45/30/15/0]_s$

INTERLAMINAR SHEARING STRESSES

Laminated composite materials have relatively weak interlaminar shear strength, the load being sustained primarily by the resin or matrix at the ply interfaces. The CLT assumes that points lying initially on a normal-to-the-middle plane of the beam remain normal-to-the-middle surface of the beam after bending. This is one of the same assumptions used in the development of small deflection theory of thin plates.[3] This assumption is equivalent to ignoring shearing strains in planes perpendicular to the middle surface of the laminate. This also means that the entire laminate is treated as a single continuous layer with linear through-the-thickness strain variation. This is known as the Kirchoff hypothesis.[4] For laminated beam analysis, this implies that the interlaminar shear stress σ_{xz} cannot be calculated from the laminate stress-strain relationships. Instead, we must rely on the equations of motion (equilibrium) of classical theory of elasticity for the determination of these stresses.

The first equation of motion can be expressed in terms of Cartesian stress components as

$$\frac{\partial \sigma_x}{\partial x} + \frac{\partial \sigma_{xy}}{\partial y} + \frac{\partial \sigma_{xz}}{\partial z} + \rho b_x = \rho f_x \ , \tag{19}$$

where b_x are external body forces and f_x are acceleration forces. For the static problems analyzed, these forces will be neglected. The resulting equation of equilibrium becomes

$$\frac{\partial \sigma_x}{\partial x} + \frac{\partial \sigma_{xy}}{\partial y} + \frac{\partial \sigma_{xz}}{\partial z} = 0 \ . \tag{20}$$

Since the beams under investigation are loaded with an evenly distributed load at the tip and since the length-to-width ratio of these beams is large, the variation of the in-plane shearing stress σ_{xy} across the width dimension y is negligible. Equation (20) can now be expressed as

$$\frac{\partial \sigma_x}{\partial x} + \frac{\partial \sigma_{xz}}{\partial z} = 0 \ . \tag{21}$$

Equation (21) can be solved for σ_{xz} in the following manner:

$$\sigma_{xz} = -\int_z \frac{\partial \sigma_x}{\partial x} dz \ . \tag{22}$$

One should notice in equation (22) that if σ_x is a linear function of x, the derivative $\partial \sigma_x / \partial x$ is constant. This implies that σ_{xz} would be a function of the thickness coordinate z only . This would be the case if the cross sections of the beams under investigation were constant. Since the investigation deals with beams of linearly varying width and thickness, the nonlinear variation of σ_{xz} as a function of length must be considered. Following Timoshenko[5] and Gere and Timoshenko,[6] the appropriate expression for σ_{xz} can be derived. Assuming that the beam of rectangular cross section in figure 11 does not have high rate of change in cross sectional thickness and width, the magnitude of the shearing stresses can be calculated by applying the same method used for prismatic beams.

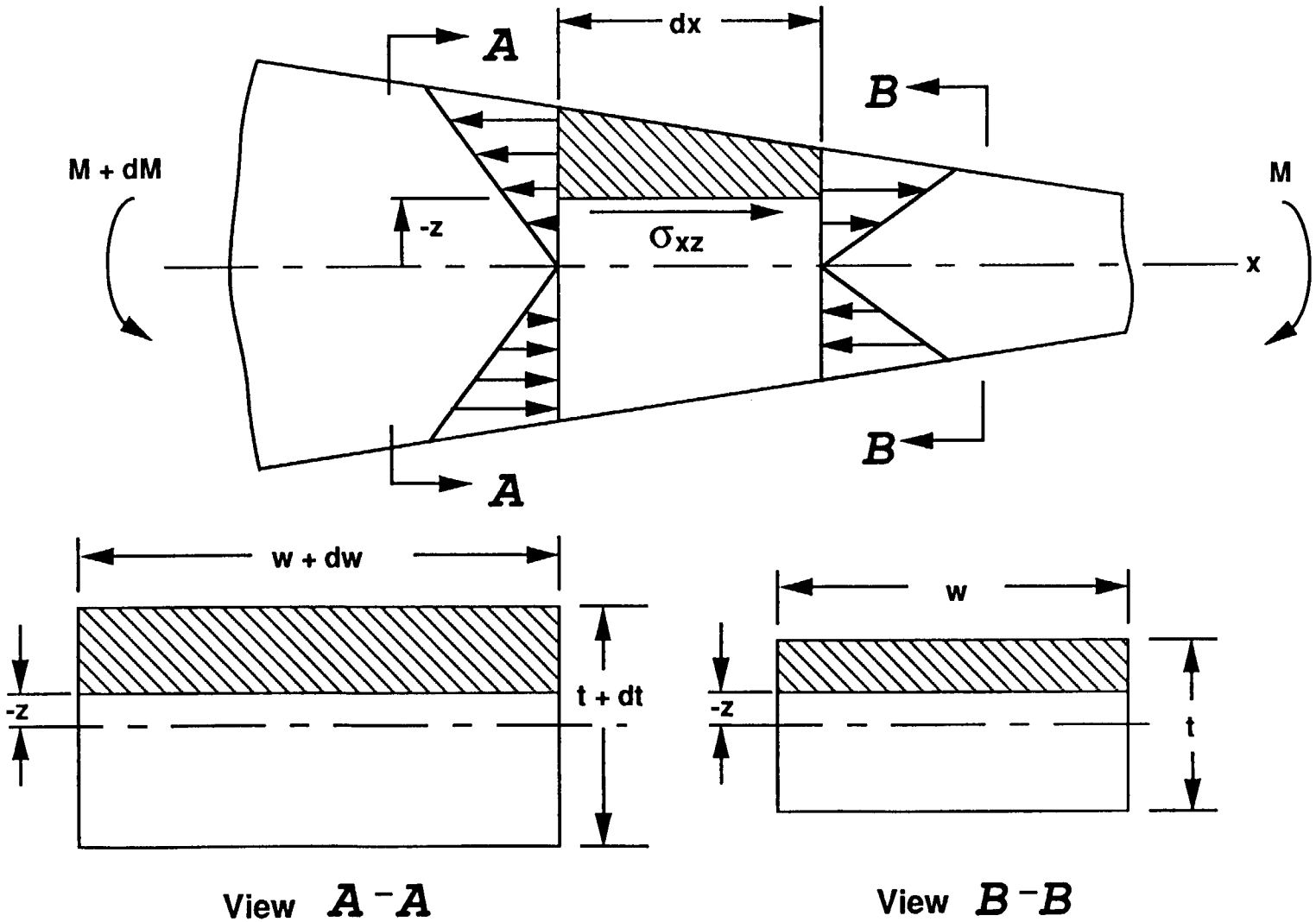

Figure 11. Element of area for transverse shear stress determination.

Summation of forces in the x direction leads to the following equation of equilibrium of the shaded element,

$$\sigma_{xz}\left(w+\frac{dw}{2}\right)dx=\int_{-z_1}^{-\frac{(t+dt)}{2}}(\sigma_x+d\sigma_x)(w+dw)dz-\int_{-z_1}^{-\frac{t}{2}}(\sigma_x w)dz\ . \tag{23}$$

In equations (23) through (36), w is a width variable and not a deflection. Expanding equation (23) and neglecting products of small differential quantities, one obtains

$$\sigma_{xz}wdx=w\int_{-z_1}^{-\frac{(t+dt)}{2}}\left(\sigma_x+\frac{d\sigma_x}{dx}dx\right)dz+\int_{-z_1}^{-\frac{(t+dt)}{2}}(\sigma_x dw)dz-\int_{-z_1}^{-\frac{(t)}{2}}(\sigma_x w)dz\ . \tag{24}$$

The expression for bending stress for the kth ply is obtained in a similar manner as equations (17) and (18)

$$\sigma_x^{(k)}=z^{(k)}M_x\left(\bar{Q}_{11}^{(k)}D_{11}^*+\bar{Q}_{12}^{(k)}D_{12}^*+\bar{Q}_{16}^{(k)}D_{16}^*\right)\ . \tag{25}$$

The quantity in the parenthesis is expressed in condensed notation as $(QD_x)^{(k)}$, and equation (25) is rewritten as

$$\sigma_x^{(k)}=z^{(k)}M_x(QD_x)^{(k)}\ . \tag{26}$$

The quantity in the parenthesis of the first integral in equation (24) can be expressed as

$$\left(\sigma_x+\frac{d\sigma_x}{dx}dx\right)=z^{(k)}\left\{M_x(QD_x)^{(k)}+\frac{d[M_x(QD_x)^{(k)}]}{dx}dx\right\}\ . \tag{27}$$

The integral can now be expressed as

$$w\int_{-z^{(k)}}^{-\frac{(t+dt)}{2}}z\left\{M_x(QD_x)^{(k)}+\frac{d[M_x(QD_x)^{(k)}}{dx}dz\right\}\ . \tag{28}$$

Performing the necessary integration and neglecting products of small differential quantities, one obtains the following expression:

$$\frac{wt^2}{8}M_x(QD_x)^{(k)}+\frac{wtdt}{4}[M_x(QD_x)^{(k)}]-\frac{w[z^{(k)}]^2}{2}[M_x(QD_x)^{(k)}]+\frac{wt^2}{8}\frac{d[M_x(QD_x)^{(k)}]}{dx}dx$$
$$-\frac{w[z^{(k)}]^2}{2}\frac{d[M_x(QD_x)^{(k)}]}{dx}dx\ . \tag{29}$$

Substituting equation (26) into the second integral on the right-hand side of equation (24) and performing the necessary integration yields the following expression after neglecting products of small differential quantities:

$$\frac{t^2dw}{8}[M_x(QD_x)^{(k)}]-\frac{[z^{(k)}]^2dw}{2}[M_x(QD_x)^{(k)}]\ . \tag{30}$$

Following this same procedure, the third integral on the right-hand side of equation (24) becomes

$$\frac{t^2 w}{8}\left[M_x(QD_x)^{(k)}\right] - \frac{[z^{(k)}]^2 w}{2}\left[M_x(QD_x)^{(k)}\right] . \tag{31}$$

Adding expressions (29), (30), and (31) according to equation (24), one obtains the following:

$$\sigma_{xz} w dx = \frac{wt}{4}\left[M_x(QD_x)^{(k)}\right]dt + \frac{wt^2}{8}\frac{d[M_x(QD_x)^{(k)}]}{dx}dx - \frac{w[z^{(k)}]^2}{2}\frac{d[M_x(QD_x)^{(k)}]}{dx}dx + \frac{t^2}{8}\left[M_x(QD_x)^{(k)}\right]dw - \frac{[z^{(k)}]^2}{2}\left[M_x(QD_x)^{(k)}\right]dw . \tag{32}$$

Solving for σ_{xz}, the following is obtained:

$$\sigma_{xz}^{(k)} = \frac{t}{4}\left[M_x(QD_x)^{(k)}\right]\frac{dt}{dx} + \left(\frac{t^2}{8} - \frac{[z^{(k)}]^2}{2}\right)\left[\frac{d[M_x(QD_x)^{(k)}]}{dx} + \frac{M_x(QD_x)^{(k)}}{w}\frac{dw}{dx}\right] . \tag{33}$$

For the beams under analysis, both the width and thickness are linear functions of x according to

$$t(x) = t_1 x + t_2 , \tag{34a}$$

$$w(x) = w_1 x + w_2 , \tag{34b}$$

where

$$t_1 = \frac{t_e - t_b}{L} \qquad t_2 = t_b ,$$

$$w_1 = \frac{w_e - w_b}{L} \qquad w_2 = w_b .$$

Taking the derivatives of equations (34) with respect to x leads to

$$\frac{dt}{dx} = t_1 = \frac{t_e - t_b}{L} , \tag{35a}$$

$$\frac{dw}{dx} = w_1 = \frac{w_e - w_b}{L} . \tag{35b}$$

Substituting the results of equations (35) into equation (33) yields the final expression for interlaminar shear stress for the kth ply.

$$\sigma_{xz}^{(k)} = \frac{t_1(t_1 x + t_2)}{4}\left[M_x(QD_x)^{(k)}\right] + \left[\frac{(t_1 x + t_2)^2}{8} - \frac{[z^{(k)}]^2}{2}\right]\left\{\frac{d[M_x(QD_x)^{(k)}]}{dx} + \frac{w_1}{w_1 x + w_2}\left[M_x(QD_x)^{(k)}\right]\right\} . \tag{36}$$

One should notice that equation (36) gives the value of σ_{xz} at any location along the length x and through the thickness z of the laminated beam. Due to limitations in the validity of equation (36) for large values of width-to-thickness ratio[7 8 9] and because for small values of this ratio, stress singularities at the free edges can cause delaminations;[10 11] our studies are limited to $6 \le w/t \le 10$.

As observed by Whitney,[11] the interlaminar shear stress variation through the thickness of the laminate is highly dependent on the lamina stacking sequence. Figure 12 shows a comparison between the transverse shear stress for two orthotropic beams; $[90/45/30/15/0/0]_s$ and $[0_6]_s$. Both beams have the same geometry and material; however, only the $[0_6]_s$ laminate produces the stress distribution which is typical for the fixed end of a doubly tapered cantilever beam. If the material were isotropic, this stress distribution would be similar to the $[0_6]_s$ laminate. Figures 13 through 15 show these stresses as calculated at various locations along the length of the beam. One should notice how, in all cases, the $[90/45/30/15/0/0]_s$ develops considerably higher stresses. It is also of interest to note that at $x = 29.25$, where the tapered beam consists of only $[0_2]_s$ plies, the shape of the distribution follows the classical sense for both laminates. This is to be expected since there is no stiffness mismatch between plies at this location.

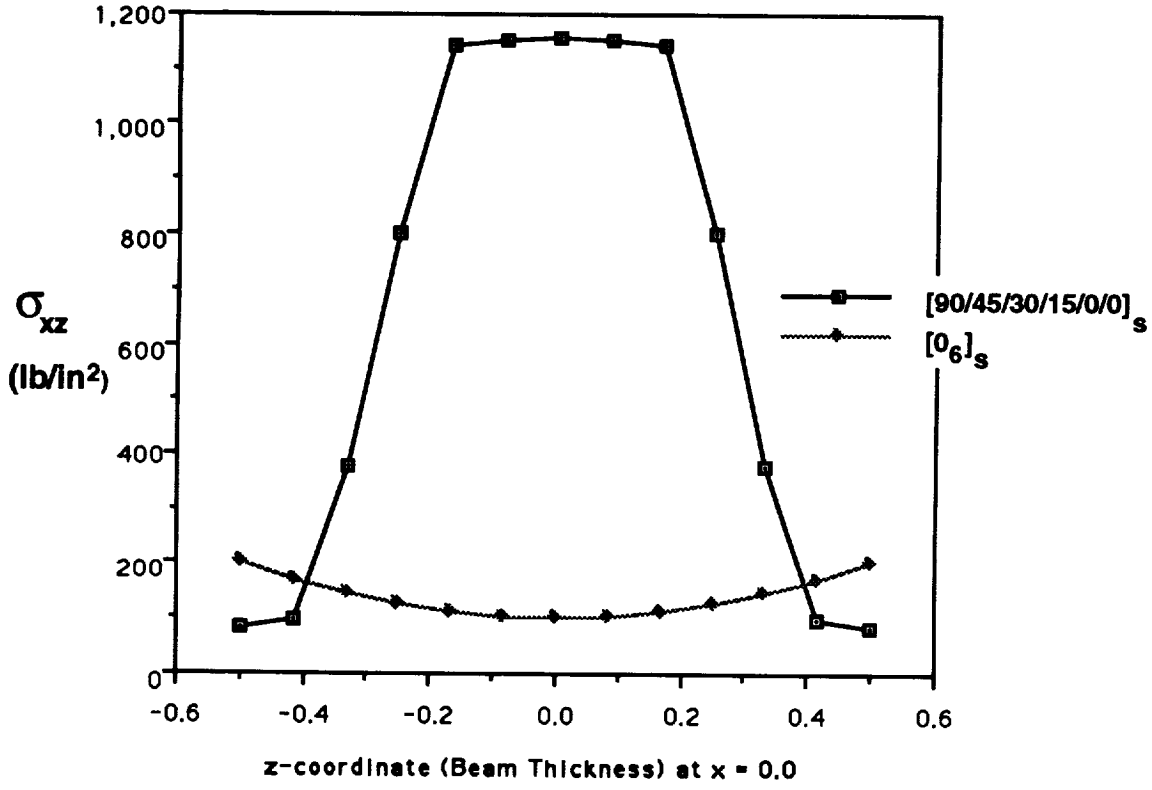

Figure 12. Transverse shear stress comparison for tapered beams (orthotropic versus isotropic).

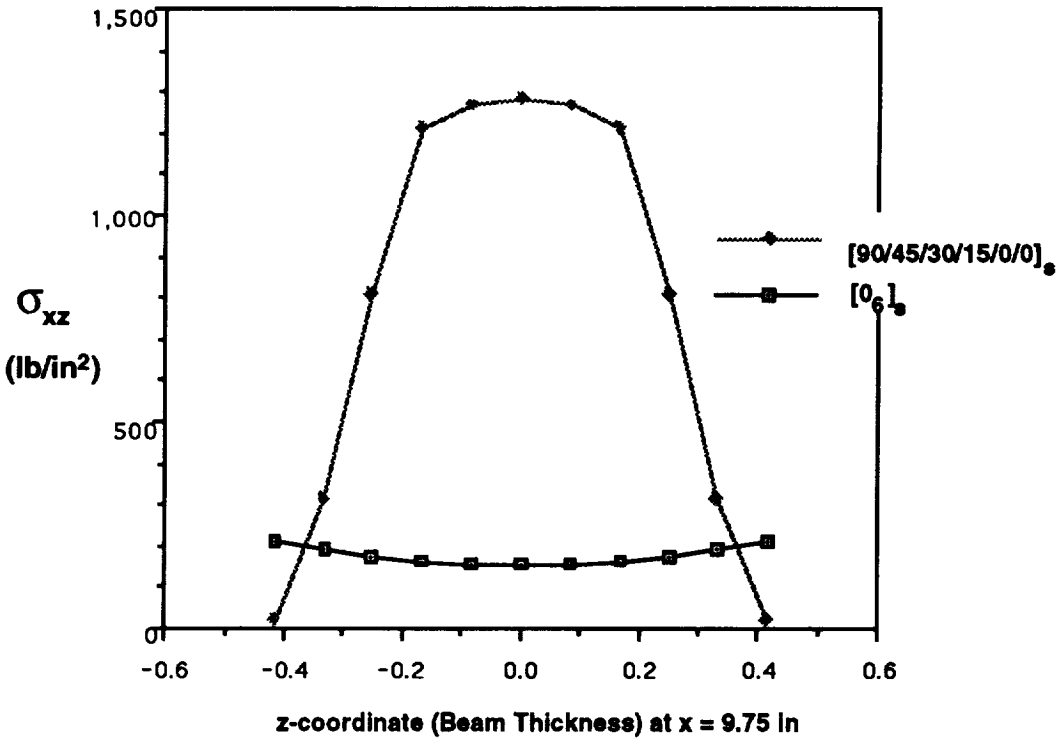

Figure 13. Transverse shear stress comparison for tapered beams (orthotropic versus isotropic).

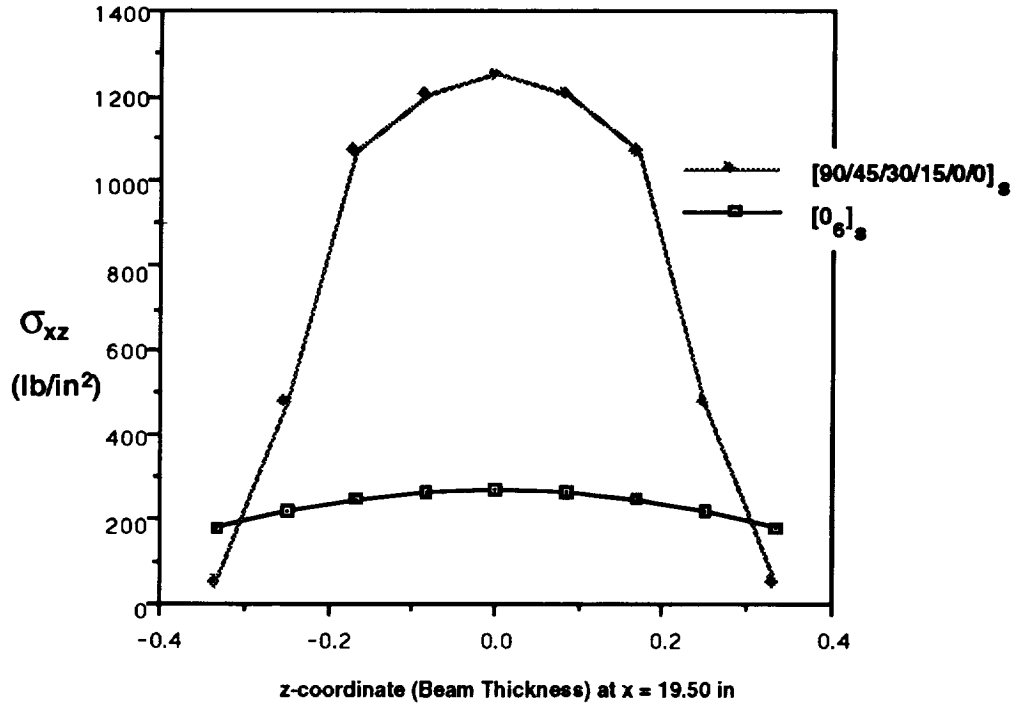

Figure 14. Transverse shear stress comparison for tapered beams (orthotropic versus isotropic).

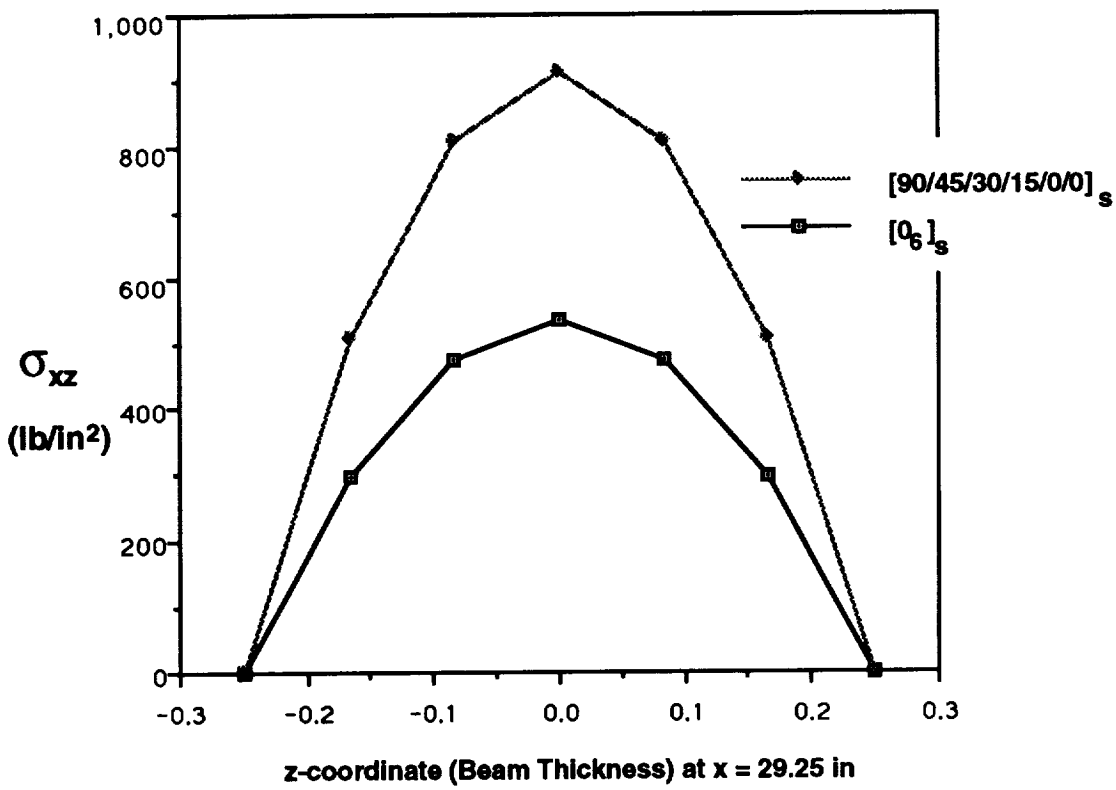

Figure 15. Transverse shear stress comparison for tapered beams (orthotropic versus isotropic).

As a direct result of the variation in stiffness along the length of the beam and because certain plies taper off to zero thickness at specific locations, there can be significant differences in stress on either side of the point where a ply "tapers off." It has been seen that the greater the difference between the ply layup angle of two adjacent plies, the greater this difference in stress. Figure 16 shows a comparison of the outermost ply bending stresses for three laminates. These are,

a. $[45_5]_s$

b. $[45/90/80/60/45]_s$

c. $[80/90/45/60/45]_s$.

The geometry and material properties are the same as the beams previously investigated. One should notice that the only difference in *b* and *c* is the interchange of the 80° and 45° plies. These plies have a difference in ply layup angle with the 90° ply of 10° and 45° respectively. It is evident that for both cases *b* and *c*, the greatest difference in stresses at the point where a ply tapers off occurs at the 45/90 or 90/45 interface. Also, the magnitude of the largest value of stress is considerably smaller for the *c* laminate. This is an important observation since the overall spring rate for both the *b* and *c* laminates changes very little. A summary is presented in table 2.

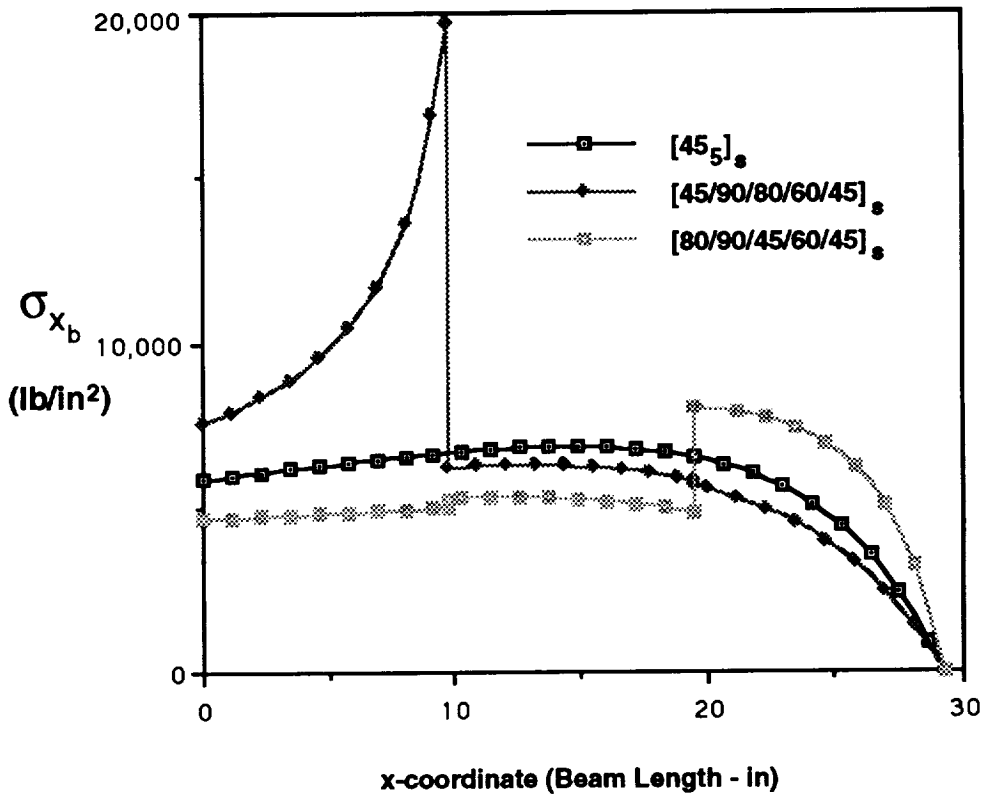

Figure 16. Outermost ply bending stress comparison for three orthotropic laminates.

Table 2. Summary of stress and stiffness for tapered beam (top ply only) (200 lb applied load).

Laminate	Max. Bending Stress (lb/in^2)	Spring Rate (lb/in)
$[45_5]_s$	6,821	53.62
$[45/90/80/60/45]_s$	19,711	56.98
$[80/90/45/60/45]_s$	8,010	61.35

It is seen that a reduction in maximum bending stress of 59 percent occurs by simply changing the location of the 45° and 80° plies. The spring rate, however, increases by only 7.6 percent. Figure 17 shows a comparison plot of the bending stiffness component D_{11} for the *b* and *c* laminates. It is relatively straight forward to see that the effect of the tapering plies on the *b* laminate is considerably greater. This is evident by the higher rate of change of the stiffness over the first 10 inches of the beam length. Figure 17a shows the bending stiffness components D_{11}, D_{12},, and D_{16} for laminate *b*. The same discontinuity at $x = 9.75$ in is evident for all three curves.

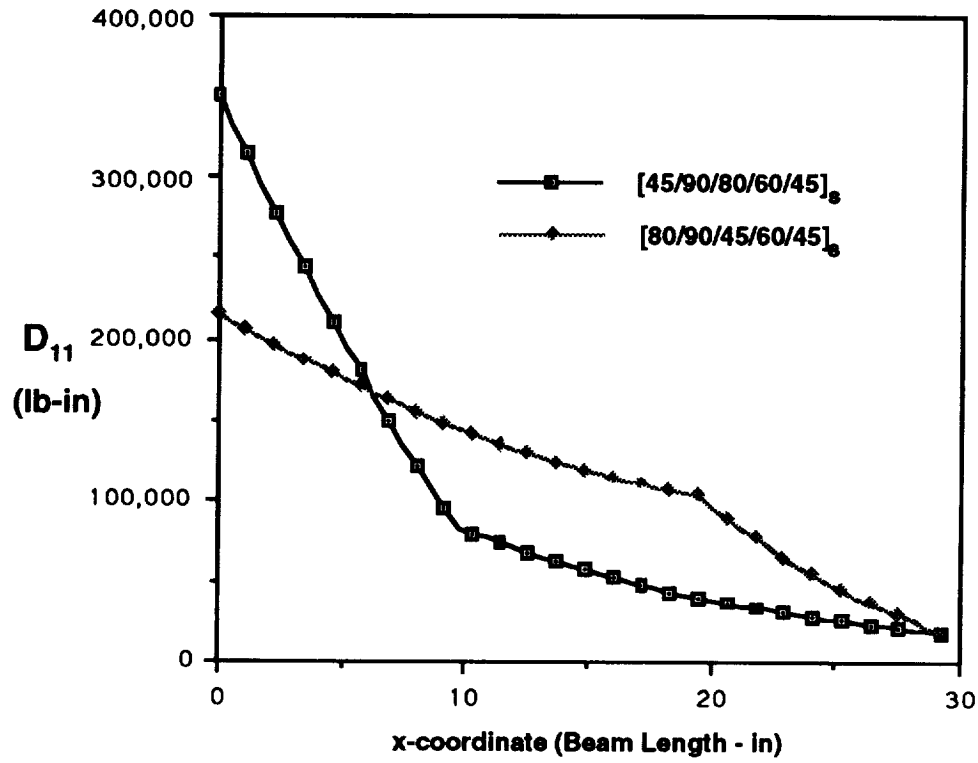

Figure 17. Bending stiffness comparison for tapered orthotropic laminated beams.

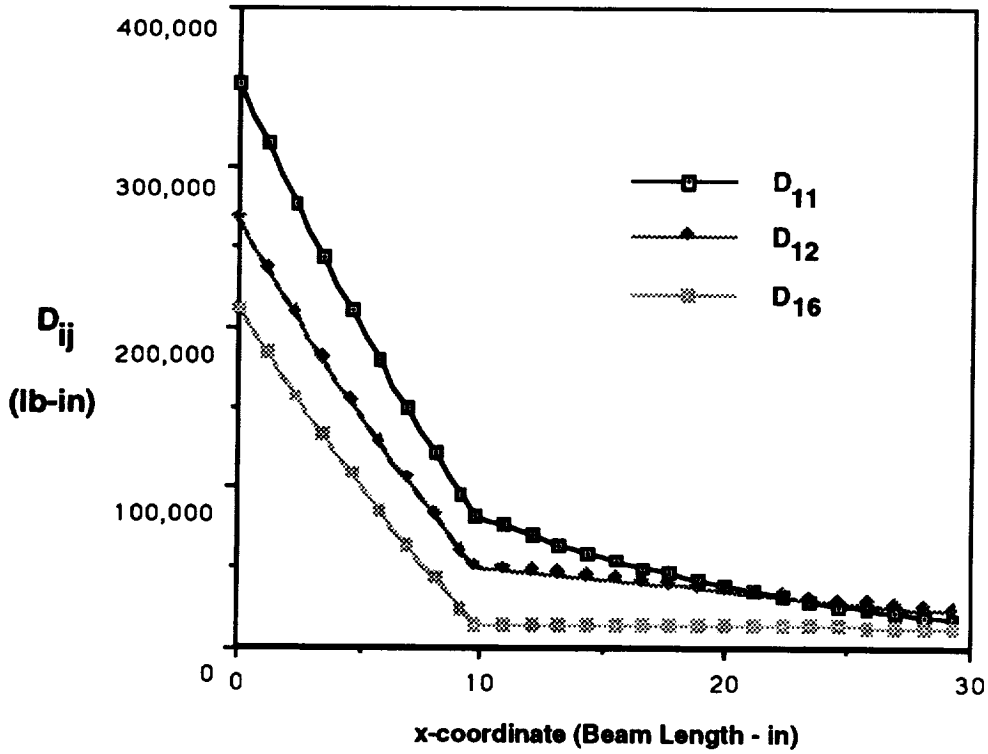

Figure 17a. Comparison of bending stiffness components D_{11}, D_{12}, and D_{16} $[45/90/80/60/45]_s$.

The D_{ij} stiffness plots can be used as an indicator for determining at which locations stresses will be highest. The following rules are proposed:

Stiffness/Stress Rules

• D_{11} curves with highest rate of change indicate highest stresses
• Sharp discontinuities, "knees," in the D_{11} curves indicate locations of highest stresses.

As an illustration, figure 18 shows the bending stress distribution along the length of the beam. One can easily notice that at the point where the top ply (45° ply) tapers off, a sharp discontinuity in stress occurs. A corresponding stress change occurs at the 90°, 80°, and 60° plies at this location.

The change in stiffness at the point where the second ply tapers off is almost negligible; likewise, the change in stress at this location (x = 19.50 in) is small (smooth transition).

From equation (22), it is evident that the transverse shear stress σ_{xz} is a direct function of the bending stress σ_{x_b}. With this knowledge, using the proposed stiffness/stress rules, one can analogously predict where the maximum interlaminar shear stresses will occur. Figure 19 shows these stresses for the three outermost (tapered) plies of the beam. One should notice how the maximum stress occurs, as expected, at the point where the first ply tapers down to zero thickness. This is also the location where the greatest stress discontinuities occur. These discontinuities, again, are due to two reasons:

- The outermost plies are tapering which contribute to a rapid increase in the compliance matrix (decrease in stiffness matrix). At the point where the ply tapers, the stiffness change is analogous to that of an isotropic beam with a sudden change in cross-sectional area.

- The difference in the layup angle between the tapering ply and the adjacent ply is greatest.

Another parameter which provides meaningful information about the relative magnitude and location of highest stresses is the nondimensional stiffness parameter (QD_x) [see equations (25) and (26)]. Figures 20 through 23 show how this parameter varies as a function of length of the beam. Figure 20 clearly shows a marked difference between the first (45°) and second (90°) plies while there is a small change between the second (90°) and third (80°) plies. In this figure, all plies are tapered which means they are the outermost plies. In figures 21 and 22, one can notice the large differences in (QD_x) for the 80-to-60 and 60-to-45 ply interfaces respectively. Large stress discontinuities would be expected at these plies based on this notion. However, one should recall that in figure 17, the bending stiffness parameter D_{11} had the highest rate of change up to the x = 9.75 in location. Between 9.75 and 29.25 in, the D_{11} parameter had a very smooth curve. This implies that in order to predict the relative location and plies that have the largest stresses, it is important to know the difference in the (QD_x) parameter between adjacent plies and the rate of change of the D_{11} bending stiffness parameter as a function of beam length. With this in mind, the magnitudes and discontinuities of the interlaminar stresses in figure 19 can be explained.

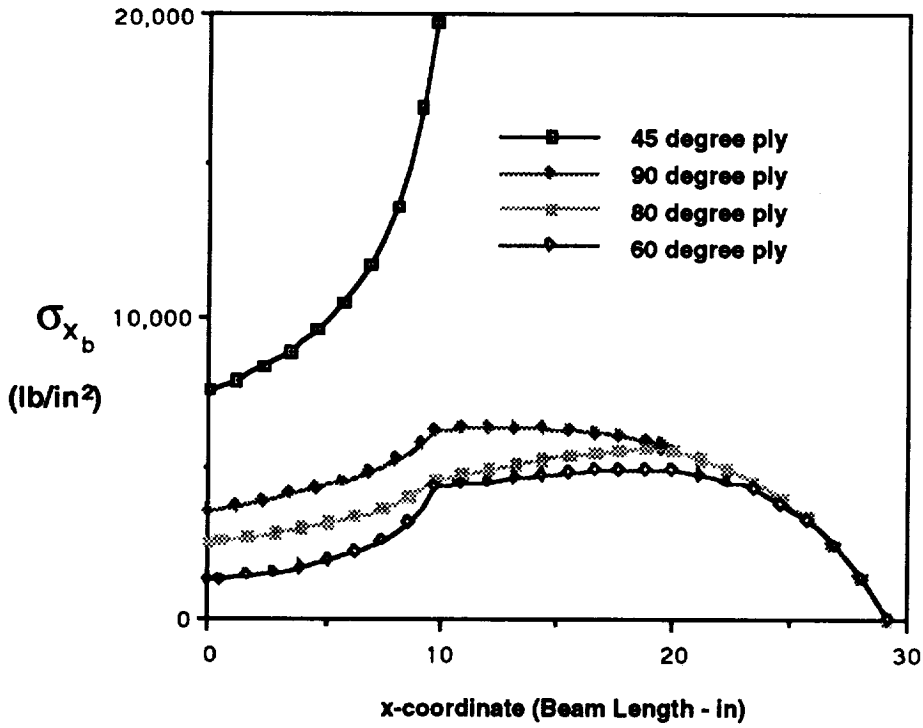

Figure 18. Bending stress distribution along the length of a tapered orthotropic laminated beam $[45/90/80/60/45]_s$.

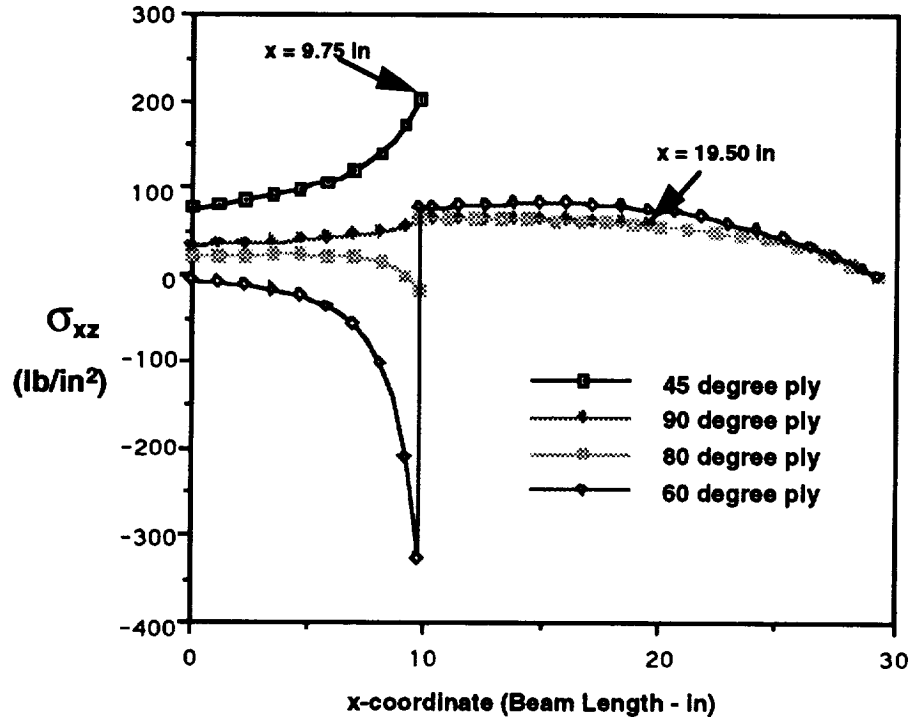

Figure 19. Interlaminar shear stress variation for tapering plies $[45/90/80/60/45]_s$.

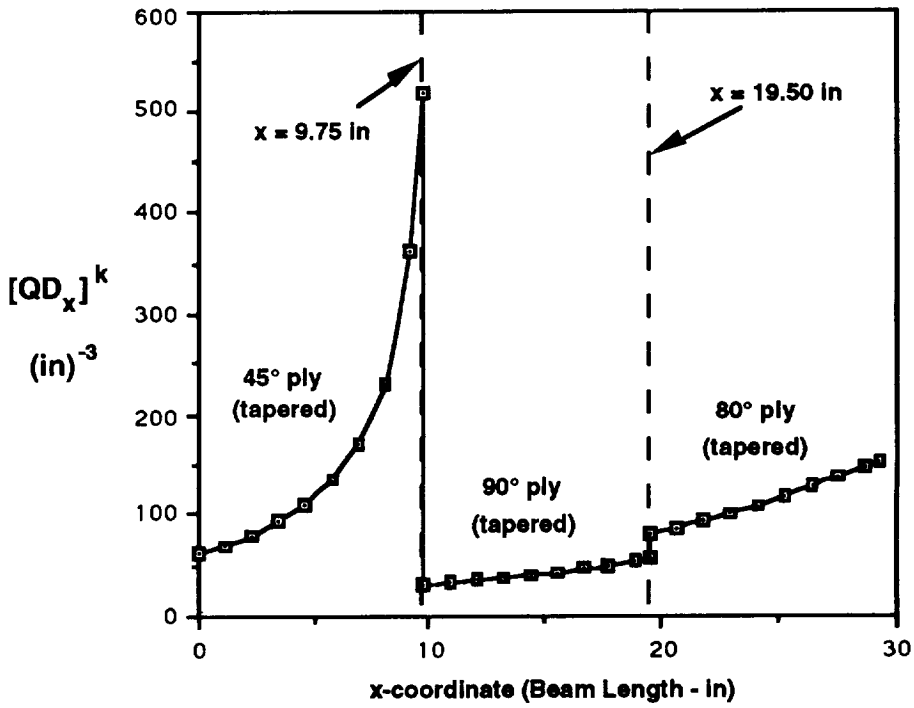

Figure 20. $[QD_x]^k$ parameter for laminated beam with tapered orthotropic plies $[45/90/80/60/45]_s$.

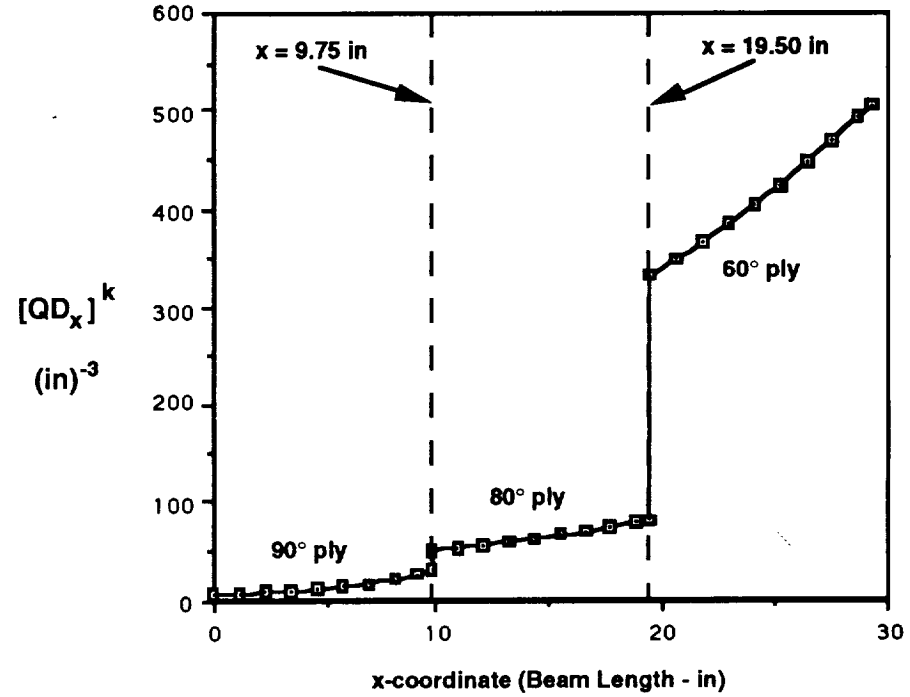

Figure 21. $[QD_x]^k$ parameter for laminated beam with tapered orthotropic plies $[45/90/80/60/45]_s$.

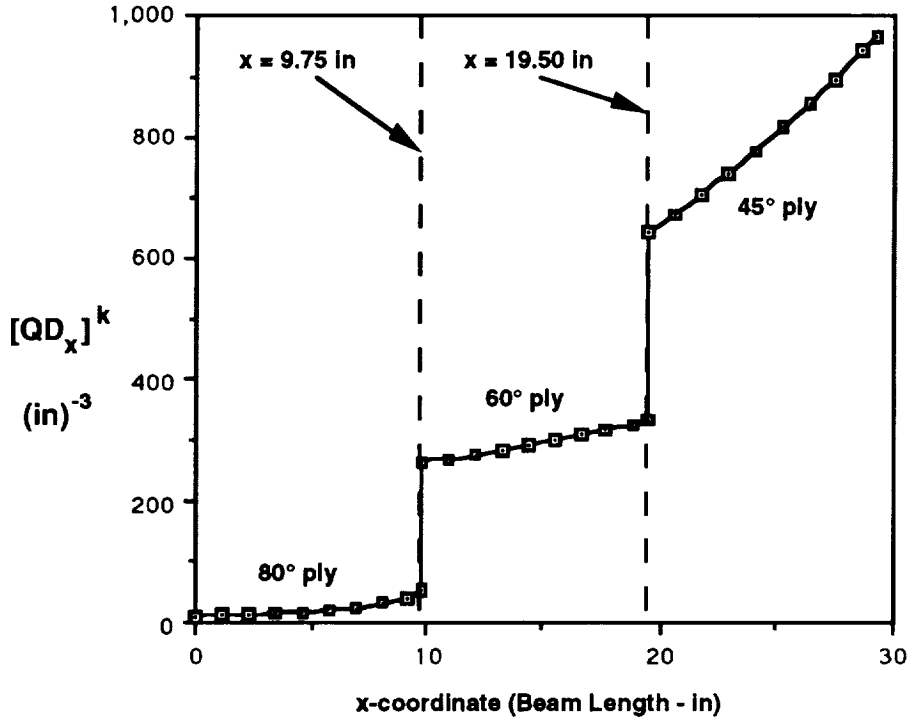

Figure 22. $[QD_x]^k$ parameter for laminated beam with tapered orthotropic plies $[45/90/80/60/45]_s$.

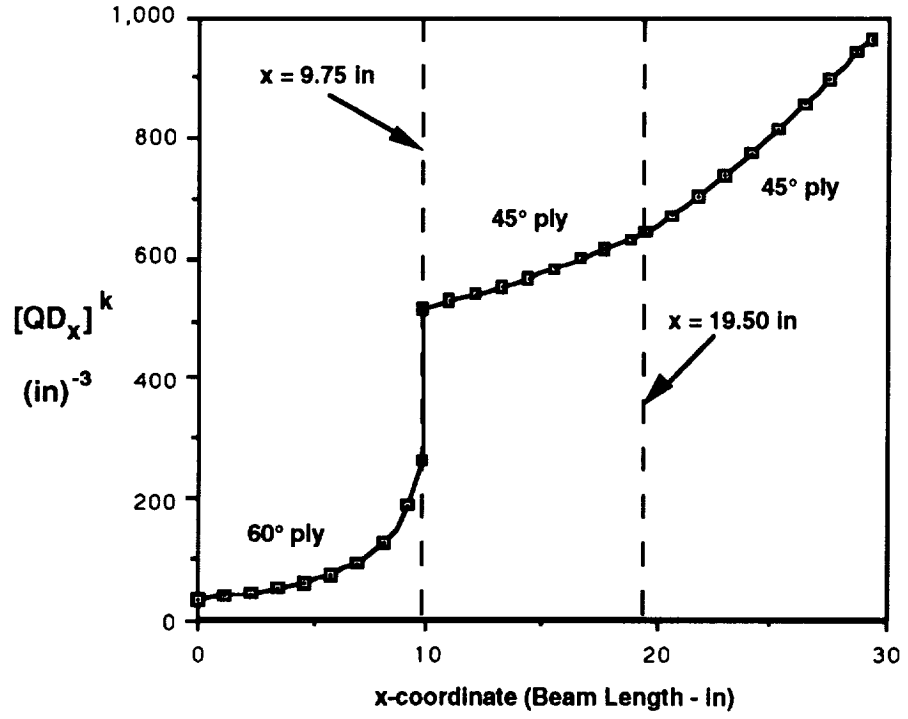

Figure 23. $[QD_x]^k$ parameter for laminated beam with tapered orthotropic plies $[45/90/80/60/45]_s$.

Since the bending stiffness parameter D_{11} has the highest discontinuity at $x = 9.75$ in, this should be the location of the highest overall stresses. This can clearly be seen in figure 19 where the differences in σ_{xz} at the $x = 19.50$ in location are considerably lower.

Figures 24 and 27 are plots of the interlaminar shear stresses between adjacent plies at the $x = 9.75$ in and $x = 19.50$ in location. These plots also show the ply angle corresponding to each lamina. Figure 24 shows a large stress difference between the 45° ply and the 90° ply at the $x = 9.75$ in location while the stress difference between the 90° and 80° plies is almost negligible. This corresponds directly to the difference in the (QD_x) parameter in figure 20 at the same locations. Figure 25 indicates a larger difference between stresses at the 80° to 60° ply interface at $x = 19.50$ in. Again this compares directly with the (QD_x) parameter difference in figure 21. The magnitude of these stresses, however, is lower because the D_{11}^* curve has approximately the same rate of change on either side of the $x = 19.50$ in location. The difference in stresses in figure 26 again corresponds to the difference in (QD_x) in figure 22. One should notice, however, that the stress between the 60° and 45° ply does not go to zero at the free end ($x = 29.25$ in) of the beam. This is because at the free end, where the load is applied, the transverse shear stress distribution allows stresses to be zero only at the outermost plies (80° to 60° interface) and not necessarily at any of the inner plies. Again figures 27 and 23 show the same relationship between σ_{xz} and (QD_x) presented in the previous plots.

SUMMARY

The design engineer must have knowledge of the effects of material and geometric properties on the magnitude and location of stresses and deformations on designed hardware during the design process. This is particularly true when designing complex components fabricated from composite materials. For the case of laminated tapered beams, the following recommendations are offered:

- The difference in ply angle between a tapering ply and the adjacent one should be as small as possible to reduce the magnitude of the bending and interlaminar shearing stresses and their discontinuities at the point where the ply "tapers off."
- A laminate should be designed so that it will produce the smallest rate of change in the bending stiffness components D_{ij}. The laminate design should produce the smoothest, although not necessarily, continuous curve possible.
- The designed laminate should exhibit the smallest differences in (QD_x) between tapering and nontapering plies.

In reading these recommendations, it is obvious that a completely isotropic beam will meet all of them. It is also noted that laminates in which all ply angles are the same also meet these recommendations. Figure 28 shows a plot of the bending components D_{11}, D_{12}, and D_{16}, for a $[30_5]_s$ laminate. There are no discontinuities in any of the curves indicating a smooth transition of stresses between tapering and adjacent plies. One should notice however that the rate of change of these curves decreases towards the tip of the beam. This along with the fact that the bending moment per unit width (fig. 29) increases toward the fixed end of the beam indicates that the highest stresses are to be expected toward this end. Another interesting plot is figure 30 where (QD_x) plots for the $[30_5]_s$ laminate are all identical. This is to be expected since all plies have the same transformed

reduced stiffnesses $\bar{Q}_{ij}$ and the stiffness terms D_{ij} do not produce discontinuous curves. Figure 31 shows the bending stress distribution for this laminate. It is important to note that it has the same kind of stress distribution exhibited by an isotropic multiple ply laminate (fig. 7).

Efficient and effective structural components can be manufactured with the knowledge of material and physical characteristics of the design. This study offers these design considerations for a particular class of laminated beams. Future work could possibly involve beams of more complex cross sections such as those typically used in structural design applications. Cross sections such as I, C, or H shapes can twist when bending loads are applied. Tapering such beams may result in increased warping resistance and decreased interlaminar shearing stresses. Structural optimization of the laminate can also minimize the weight while making the member structurally sound.

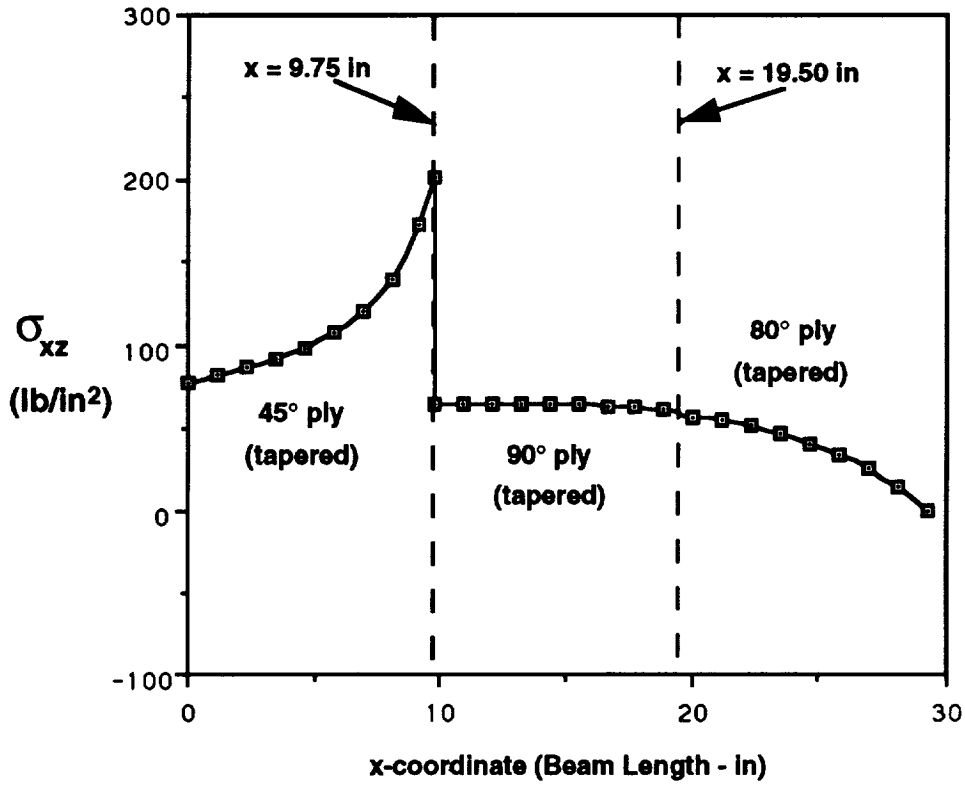

Figure 24. Interlaminar shear stress between adjacent plies $[45/90/80/60/45]_s$.

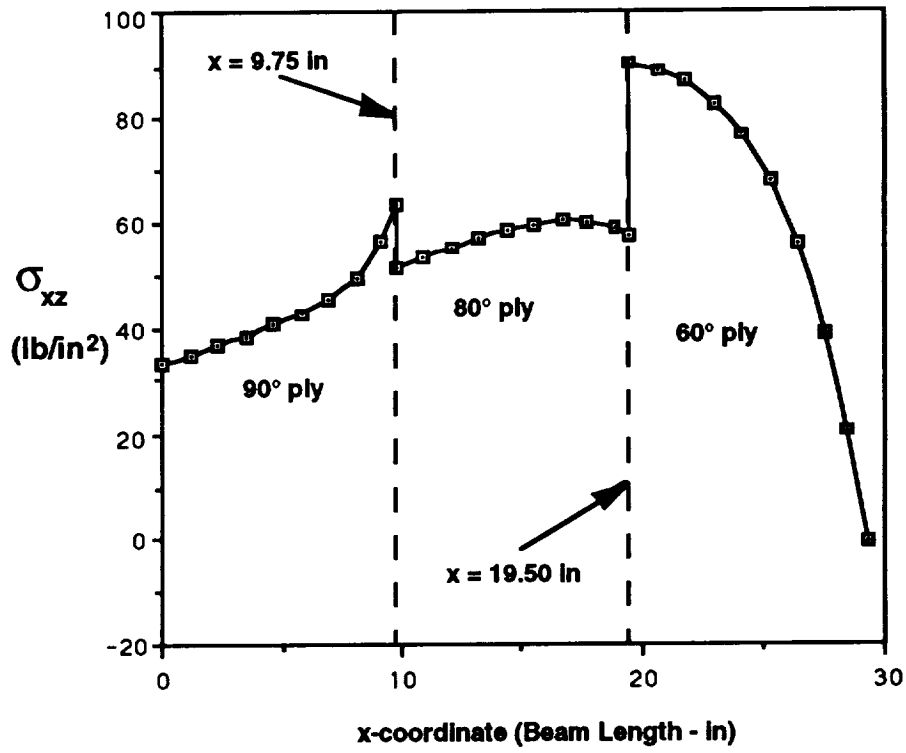

Figure 25. Interlaminar shear stress between adjacent plies $[45/90/80/60/45]_s$.

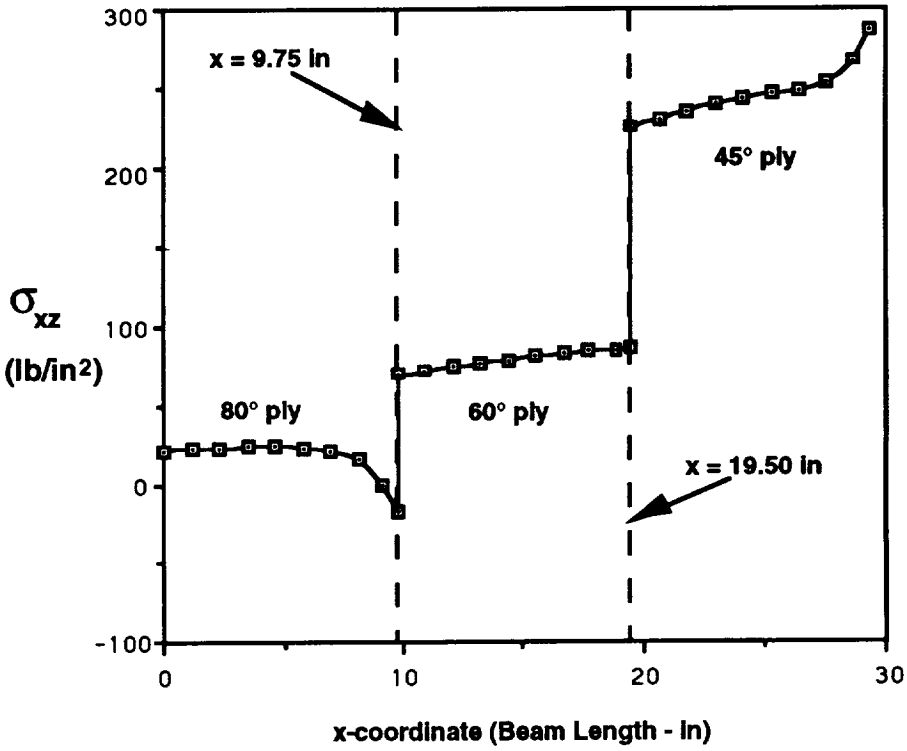

Figure 26. Interlaminar shear stress between adjacent plies $[45/90/80/60/45]_s$.

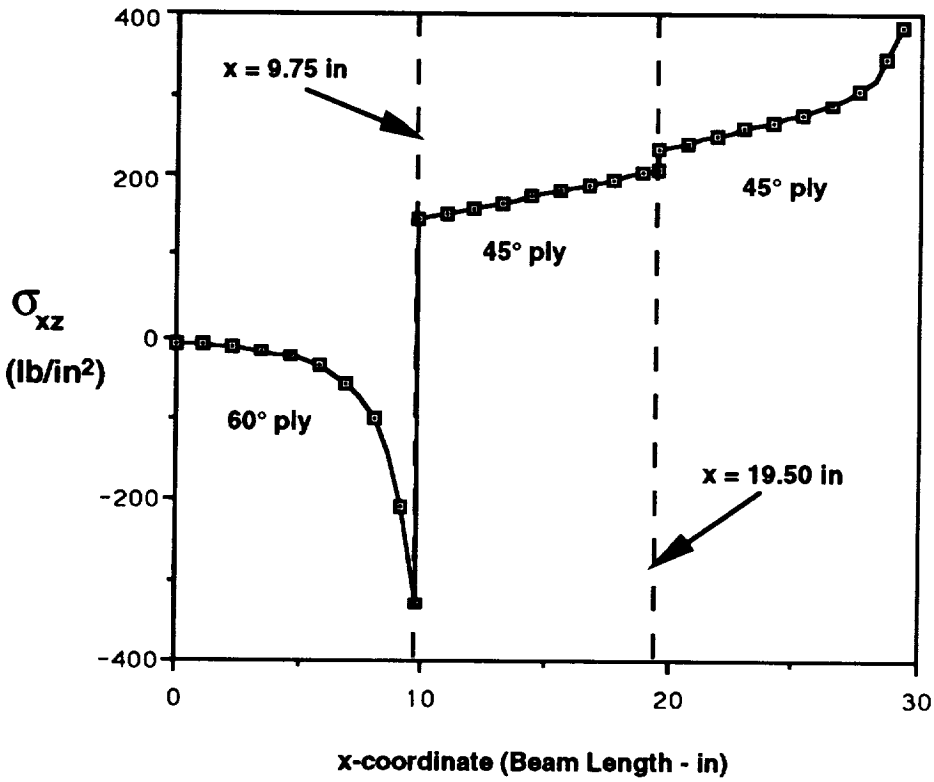

Figure 27. Interlaminar shear stress between adjacent plies $[45/90/80/60/45]_s$.

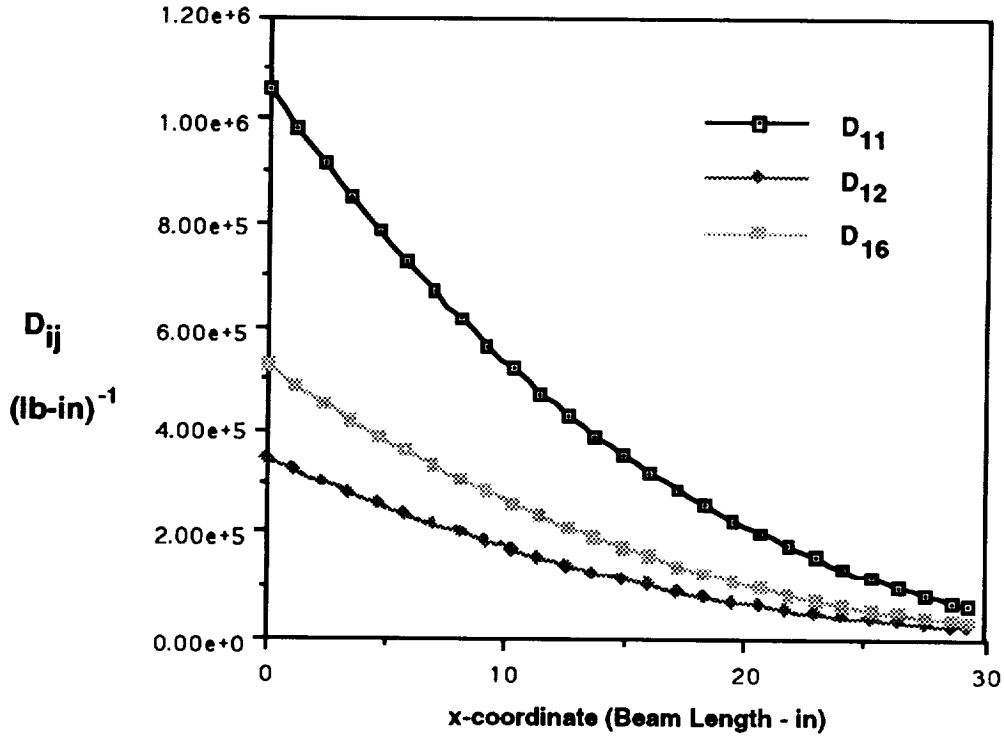

Figure 28. Comparison of bending stiffness components D_{11}, D_{12}, and D_{16} $[30_5]_s$.

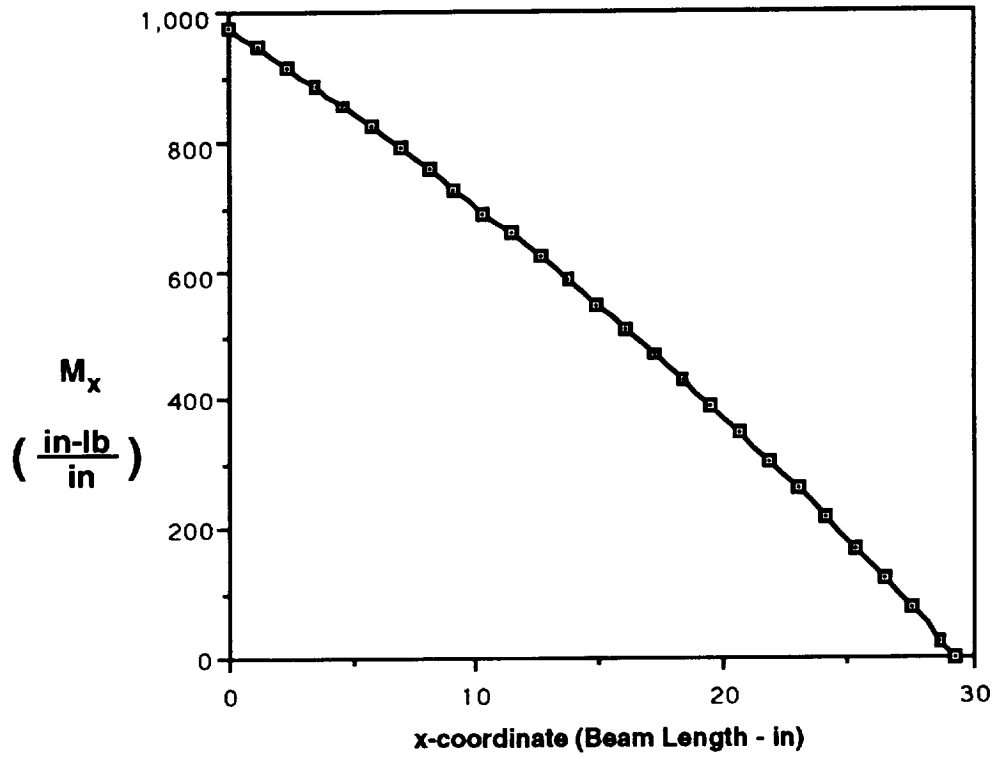

Figure 29. Bending moment per unit width for a tapered beam.

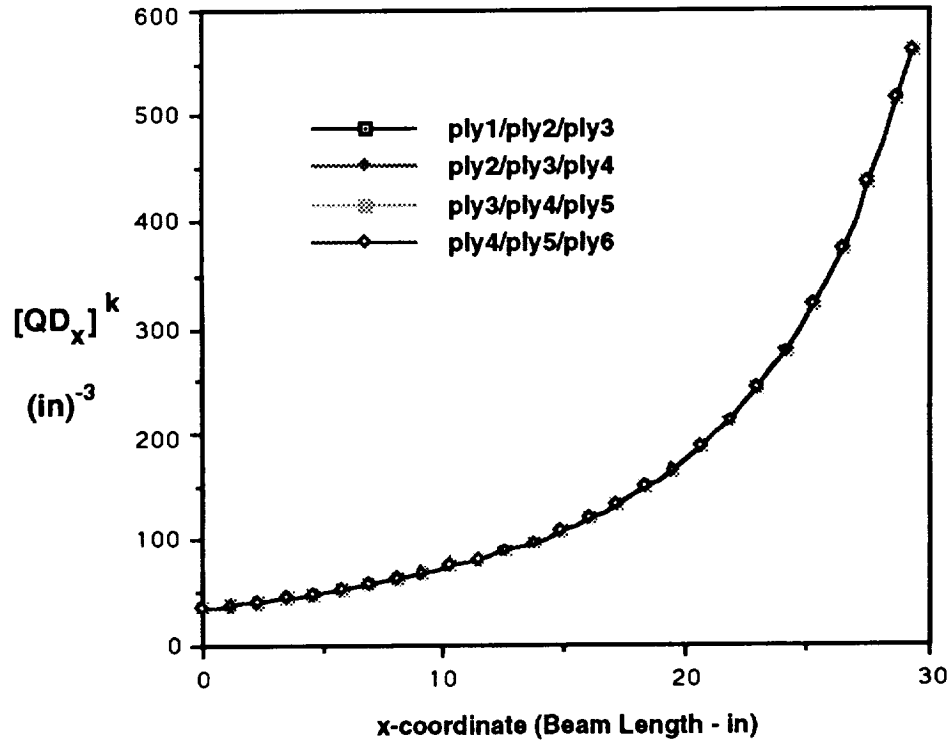

Figure 30. $[QD_x]^k$ parameter for laminated beam with tapered orthotropic plies $[30_5]_s$.

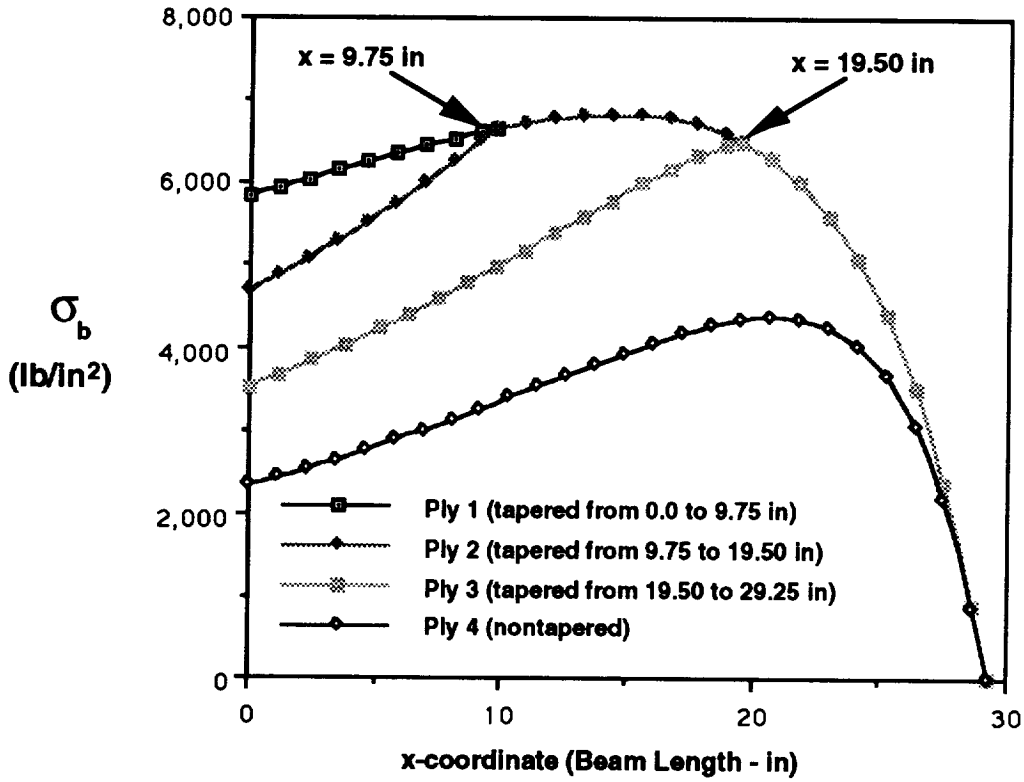

Figure 31. Bending stress versus beam length $[30_5]_s$.

REFERENCES

1. Rodriguez, P.I. and Bower, M.V.: "Optimum Design of A Linearly Tapered Laminated Cantilever Beam." Optimization of Structural Systems and Industrial Applications, Second International Conference on Computer Aided Optimum Design of Structures (OPTI '91), Boston, MA.

2. Whitney, J.M.: "The Effect of Transverse Shear Deformation on the Bending of Laminated Plates." Journal of Composite Materials, vol. 3, 1969, pp. 534–547.

3. Timoshenko, S., and Woinowsky-Krieger, S.: "Theory of Plates and Shells" (Second Edition). McGraw-Hill Book Company, New York, NY, 1959.

4. Jones, R.M.: "Mechanics of Composite Materials." McGraw-Hill Book Company, Washington, DC, 1975.

5. Timoshenko, S.: "Strength of Materials (Part II), Advanced Theory and Problems" (Third Edition). D. Van Nostrand Company Inc., Princeton, NJ, 1956.

6. Gere, J.M., and Timoshenko, S.: "Mechanics of Materials" (Third Edition). PWS-Kent Publishing Co., Boston, MA, 1972.

7. Carter, W.J.: "Torsion and Flexure of Slender Solid Sections." Journal of Applied Mechanics, vol. 25, March 1958, pp. 115–121.

8. Hopkins, B.R.: "Design Analysis of Shafts and Beams." McGraw-Hill Book Company, New York, NY, 1970.

9. Timoshenko, S.P., and Goodier, J.N.: "Theory of Elasticity" (Third Edition). McGraw Hill Book Company, New York, NY, 1970.

10. Pipes, R.B., and Pagano, N.J.: "Interlaminar Stresses in Composite Laminates Under Uniform Axial Extension." Journal of Composite Materials, vol. 4, 1970, pp. 538–548.

11. Whitney, J.M.: "Structural Analysis of Laminated Anisotropic Plates." Technomic Publishing Co., PA, 1987.

APPROVAL

DESIGN OF MULTIPLE-PLY LAMINATED COMPOSITE TAPERED BEAMS

By P. Rodriguez

The information in this report has been reviewed for technical content. Review of any information concerning Department of Defense or nuclear energy activities or programs has been made by the MSFC Security Classification Officer. This report, in its entirety, has been determined to be unclassified.

J.C. BLAIR
Director, Structures and Dynamics Laboratory

☆ U.S. GOVERNMENT PRINTING OFFICE 1993–733-050/80088